0026-895X/05/6805-1439–1454$20.00
MOLECULAR PHARMACOLOGY
Copyright © 2005 The American Society for Pharmacology and Experimental Therapeutics
Mol Pharmacol 68:1439–1454, 2005

Vol. 68, No. 5
14910/3059691
Printed in U.S.A.

Protein PEGylation Decreases Observed Target Association Rates via a Dual Blocking Mechanism[S]

Susanne Kubetzko, Casim A. Sarkar, and Andreas Plückthun

Department of Biochemistry (S.K., C.A.S., A.P.), and Department of Oncology (S.K.), University Hospital, University of Zürich, Zürich, Switzerland

Received May 18, 2005; accepted August 11, 2005

ABSTRACT

PEGylation is an attractive strategy to enhance the therapeutic efficacy of proteins with a short serum half-life. It can be used to extend the serum persistence and to reduce the immunogenicity of proteins. However, PEGylation can also lead to a decrease in the functional activity of the molecule to which it is applied. We constructed site-specifically PEGylated variants of anti-p185^{HER-2} antibody fragments in the format of a monovalent single-chain variable fragment and a divalent miniantibody and characterized the antigen binding properties in detail. Mass-transport limited BIAcore measurements and binding assays on HER-2-overexpressing cells demonstrated that the immunoreactivity of the antibody fragments is fully maintained after PEGylation. Nevertheless, we found that the attachment of a 20-kDa polyethylene glycol (PEG) moiety led to a reduction in apparent affinity of approximately 5-fold, although in both formats, the attachment site was most distal to the antigen binding regions. This decrease in affinity was observed in kinetic BIAcore measurements as well as in equilibrium binding assays on whole cells. By analysis of the binding kinetics, we could pinpoint this reduction exclusively to slower apparent on rates. Through both experimental and computational analyses, we demonstrate that these reduced on-rates do not arise from diffusion limitations. We show that a mathematical model accounting for both intramolecular and intermolecular blocking mechanisms of the PEG moiety can robustly explain the observed binding kinetics. The results suggest that PEGylation can significantly alter the binding-competent fraction of both ligands and receptors and may help to explain some of the beneficial effects of PEGylation in vivo.

PEGylation is one of the best validated strategies to extend the serum half-life of therapeutic agents and to decrease their immunogenicity (Bailon et al., 2001; Greenwald et al., 2003). There are six different FDA-approved drugs based on PEGylated proteins on the market, and several more are undergoing clinical trials (Greenwald et al., 2003; Harris and Chess, 2003; Marshall et al., 2003). In this strategy, a polyethylene glycol (PEG) moiety is covalently attached to the therapeutic protein of interest. Because of the bulky and hydrophilic nature of the PEG polymer, it enhances the hydrodynamic size of the conjugated protein far beyond the increase in molecular mass (Yang et al., 2003). Because a PEG tail is not a rigid moiety, but quite a flexible one, it can also act to shield protein sites from recognition by the immune system, cellular receptors, or proteases. These properties lead to decreased renal, enzymatic, and cellular clearance, resulting in prolonged circulation half-lives in the bloodstream (Chapman et al., 1999; Yang et al., 2003).

However, reduction or even loss of functional activity can be an unintended side effect of PEGylation if the polymer strand sterically hinders the binding of the conjugate to the target. Many PEGylated antibody fragments of the first generation encountered this problem, because at that time the PEG conjugation was performed via random attachment, most commonly through lysine residues (Chapman, 2002; Weir et al., 2002). Thereafter, site-specific PEGylation techniques were developed (Harris and Chess, 2003; King et al., 1994), in which the PEG molecule is attached to the protein at a single unpaired cysteine residue that can be engineered at a position distal to the target-binding region of the protein. Successful applications of this technique have been reported (Chapman et al., 1999; Lee et al., 1999; Weir et al., 2002), showing that PEG tails from 2 kDa up to 40 kDa can be

This work was supported in part by a Kirschstein NRSA postdoctoral fellowship from the National Institutes of Health (to C.A.S.) and a grant from the Schweizerischer Nationalfonds (3100-065344/2) (to A.P.).

S.K. and C.A.S. contributed equally to this study.

[S] The online version of this article (available at http://molpharm.aspetjournals.org) contains supplemental material.

Article, publication date, and citation information can be found at http://molpharm.aspetjournals.org.
doi:10.1124/mol.105.014910.

ABBREVIATIONS: PEG, polyethylene glycol; scFv, single-chain variable fragment; PBS, phosphate-buffered saline; BSA, bovine serum albumin; DLS, dynamic light scattering; ECD, extracellular domain; RU, resonance units; Ni-NTA, nickel nitriloacetic acid; HER-2, human epidermal growth factor receptor 2; PEG20, 20-kDa maleimide-PEG moiety.

coupled to antibody fragments (scFv or Fab). However, conflicting conclusions about changes in affinity have been reached (see below).

Because of its great potential for increasing serum half-life and decreasing immunogenicity, we chose site-specific PEGylation as a strategy to improve the pharmacokinetic behavior of antibody fragments that were generated for use in tumor targeting (S. Kubetzko, E. Balic, R. Waibel, U. Zangemeister-Wittke, and A. Plückthun, manuscript in preparation). We constructed PEGylated versions of the monovalent scFv 4D5 and the bivalent miniantibody 4D5-dhlx, which consists of the scFv 4D5 fused via a hinge region to the self-associating dimerization peptide dhlx (for review, see Willuda et al., 2001) (Fig. 1). These antibody fragments were derived from the humanized antibody 4D5 (Carter et al., 1992; for review, see Willuda et al., 2001), which binds specifically and with high affinity to the extracellular domain of $p185^{HER-2}$, a transmembrane glycoprotein that is overexpressed in 25 to 30% of breast and ovarian carcinomas (Slamon et al., 1989).

We introduced a cysteine residue, to which the PEG polymer was coupled, at the C terminus of the scFv 4D5 and the miniantibody 4D5-dhlx, separated by a glycine linker. Thus, the attachment site of PEG was placed most distal to the antigen binding regions of these antibody fragments. Nevertheless, we found a decrease in apparent affinity when comparing the binding properties of the PEGylated constructs with those of their unPEGylated equivalents. This is in contradiction to some earlier reports (Chapman et al., 1999; Lee et al., 1999; Chapman, 2002) but consistent with a more recent study (Yang et al., 2003). Earlier reports had suggested that PEGylated antibody fragments, which carry the PEG tail at a site where direct interference with the binding region is unlikely, retain full binding activity.

The conflicting views in the literature about the effect of PEGylation on binding affinity prompted us to investigate this effect in more detail. We assessed the antigen-binding properties of the different constructs on tumor cells as well as by kinetic BIAcore measurements. To be able to interpret the impact of PEG on the association and dissociation rates independently, a special effort was undertaken to determine the percentage of active molecules. Furthermore, we analyzed and compared hydrodynamic parameters (size and diffusion coefficient) of the PEGylated and the unmodified antibody fragments. This allowed us to differentiate the effects of slower diffusion from those of steric hindrance by the long mobile PEG moiety, leading to a lower percentage of successful collisions that result in binding. All together, the results of this study should help to clarify the molecular factors responsible for the change in apparent affinity upon PEGylation and their respective contributions.

Materials and Methods

Tumor Cell Line and Recombinant Antigen. For the binding experiments, we used the ovarian carcinoma cell line SK-OV-3 (HTB 77, ECACC, Salisbury, Wilts, UK). Culturing and harvesting of the cells was performed as described previously (Willuda et al., 2001). The purified recombinant antigen $p185^{HER-2}$-ECD was a kind gift from Genentech Inc. (South San Francisco, CA).

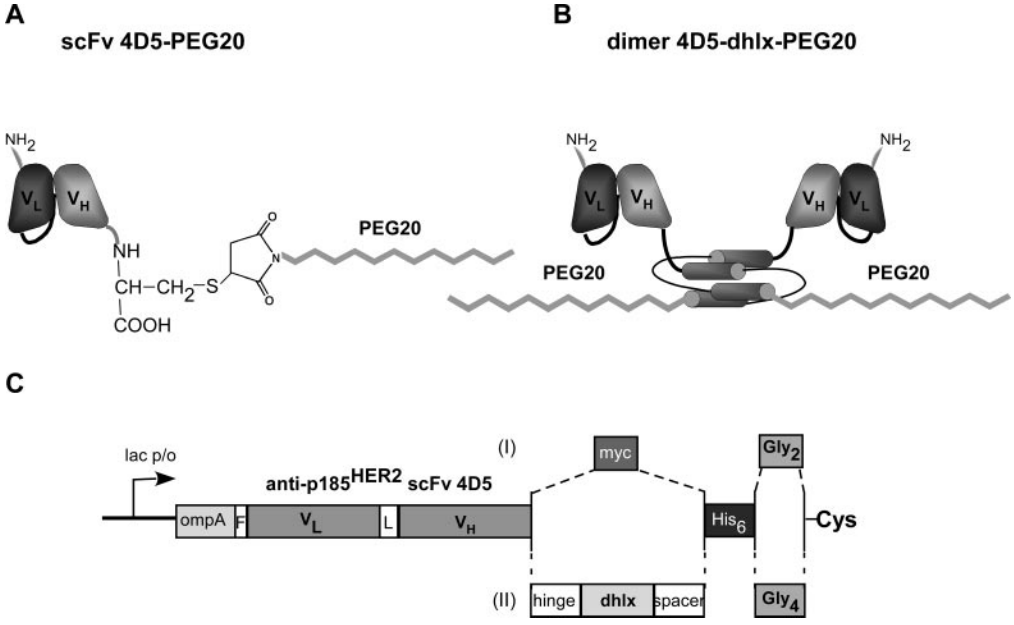

Fig. 1. Schematic representation of the molecular set up of the PEGylated antibody formats. A, PEGylated monomeric miniantibody 4D5-PEG20. The scFv 4D5, which is in the V_L-linker-V_H orientation, was site-specifically conjugated with a 20-kDa maleimide-PEG moiety (PEG20) at a single engineered cysteine residue, placed at the C terminus of the scFv fragment. Coupling was obtained by formation of a thioether bond between the free cysteine and the maleimide residue. B, PEGylated dimeric miniantibody 4D5-dhlx-PEG20. The antibody fragment 4D5-dhlx consists of the scFv 4D5 and the synthetic dhlx peptide (Hill and deGrado, 1998), which is C-terminally fused to the scFv via a hinge peptide, forms an antiparallel helix-turn-helix motif and mediates dimerization by self-association. For PEGylation, the construct carries a C-terminal cysteine and the same strategy was used as for the monomeric construct, resulting in a dimeric miniantibody with two PEG molecules attached. C, gene constructs of the modified 4D5 miniantibodies. For periplasmic expression in *E. coli*, the *lac* promoter and the *ompA* signal-peptide sequence were used. The monomeric construct (I) starts with an N-terminal short FLAG tag (F), followed by the scFv 4D5, a myc tag, and a His_6 tag. The construct terminates in a single cysteine residue, separated by a short glycine (Gly_2) linker from the His_6 tag. Instead of the myc tag, the gene construct of the dimeric antibody fragment (II) contains the dimerization domain dhlx, flanked by a murine IgG3 hinge and a GGSGGAP spacer sequence (Willuda et al., 2001). Here, the C-terminal cysteine is separated from the His_6 tag by four glycine residues.

Design, Expression, and Purification of the Constructs. The construction of the cysteine mutants, the expression of the monovalent scFv and the divalent miniantibody, and the purification of these proteins are described in the Supplemental Materials.

PEGylation of the 4D5 Miniantibodies. Purified protein samples of the monomeric (scFv 4D5-Cys) and dimeric (4D5-dhlx-Cys) miniantibodies were concentrated to approximately 0.3 to 1 mg/ml by centrifugation at 2000*g* and 4°C, using a 10-kDa cutoff microconcentrator (Ultrafree-MC low protein binding; Millipore, Billerica, MA). To enable site-specific PEGylation, the C-terminal cysteine residue was selectively reduced before incubation with maleimide-PEG20 (Nektar, Huntsville, AL). The reducing conditions had to be mild to prevent breakage of the internal disulfide bonds in the V_L and V_H domains. Therefore, the concentrated protein solution was incubated with 3 mM dithiothreitol (final concentration) for 30 min at 37°C. The excess reducing agent was then immediately removed by desalting over a Sephadex G-25 column (PD-10 or NAP-5; GE Healthcare, Little Chalfont, Buckinghamshire, UK). In this step, the buffer was also exchanged to the one used in the PEGylation reaction (100 mM citric acid, 100 mM NH_4Ac, 2 mM EDTA, pH 6.0, filtered, degassed and saturated with N_2). The PEGylation reaction was then carried out by addition of maleimide-PEG20 in 5- to 10-fold molar excess over freshly reduced protein, followed by incubation at 37°C for 2 h. The efficiency of PEGylation was analyzed by SDS-PAGE (12% gel, Coomassie-staining) and size exclusion chromatography on a Superdex 200 column with an ÄKTAexplorer system (GE Healthcare, Little Chalfont, Buckinghamshire, UK). The same chromatography system was used to purify the PEGylated proteins from both the native antibody fragments and the unreacted free PEG.

Size Exclusion Chromatography. Analytical gel filtration analysis of the unmodified and PEGylated antibody fragments was performed with an ÄKTAexplorer chromatography system at 4°C and a flow rate of 0.5 ml/min, using a Superdex-200 column (24-ml bed volume). The column was equilibrated with filtered and degassed phosphate-buffered saline (PBS), containing 1 M NaCl and 0.05% Tween 20. For calibration, five protein standards were used: β-amylase (200 kDa), alcohol dehydrogenase (150 kDa), bovine serum albumin (BSA; 66 kDa), carbonic anhydrase (29 kDa), and cytochrome *c* (12.5 kDa). Samples of the different constructs were injected at a concentration between 500 μg/ml and 1.2 mg/ml in a volume of 100 μl. The absorption was recorded at 280, 260, and 230 nm. If a low PEGylation yield (less than 80%) or impurities were detected, preparative size exclusion chromatography under the same conditions was used as an additional purification step.

Static Light Scattering Analysis. The molar masses of the different 4D5-miniantibodies were determined by multiangle static light scattering analysis and compared with the theoretically expected values. We used the tri-angle (45°, 90°, 135°) light scattering detector miniDAWN (Wyatt Technology Corporation, Santa Barbara, CA) in combination with the interferometric refractometer OPTILAB (Wyatt Technology Corporation), which were serially connected between the UV and conductivity detectors of the ÄKTAexplorer chromatography system. Thus, it was possible to perform size exclusion chromatography and determine the molar mass of every single protein peak online. The same conditions as for the gel filtration analysis were used, including filtration and degassing of the buffers, flow rate (0.5 ml/min), injection volume (100 μl) and concentration of the injected protein samples (0.5–1.2 mg/ml, sterile-filtered). Before the measurements were started, the detector system of the miniDAWN was equilibrated with the running buffer (PBS, containing 1 M NaCl and 0.05% Tween 20) for at least 2 h to ensure stable baseline signals. During the measurements, the laser scattering (690 nm), the UV absorption (280 nm), and the refractive index (690 nm) of the protein solutions were recorded. Data were evaluated with the Wyatt software ASTRA. For calculations of the molar masses, we set the refractive index of the buffer solution to 1.33, and the refractive index increment (*dn/dc*) of the proteins either to 0.166 ml/g for the PEGylated miniantibodies or to 0.185 ml/g for the unPEGylated ones.

Dynamic Light Scattering Analysis. To determine the diffusion coefficients and the hydrodynamic sizes of the PEGylated and unPEGylated miniantibodies, dynamic light scattering (DLS) analyses were performed. We used the one-angle (90°, laser wavelength 826 nm) DLS-instrument DynaPro (Viscotek, Houston, TX) and protein concentrations between 650 μg/ml and 1.3 mg/ml in PBS. Before measurements were started, the detector was equilibrated with ultra high-purity water and subsequently with PBS to ensure that the background scatter, caused by the solvent, was steady (fluctuation rate <10%) and at a low level. All solutions, including the analyzed protein samples, were filtered through a 0.1-μm filter (Whatman, Clifton, NJ) upon injection. The measurements were carried out in a 10-μl quartz cuvette at 20°C, following a schedule of 10 acquisition points in 10 min and repeated three times per analysis. Parameters for the data collection were set as follows: 10-s maximal acquisition time, a sensitivity of 100% avalanche photodiode bias (maximal intensity, 1.5×10^6 photon counts/s) and signal-to-noise threshold ratio of 1. Data were evaluated with the software DYNAMICS version 4.0 (Viscotek), using a monomodal size distribution model.

Radioimmunoassay on Human SK-OV-3 Tumor Cells. The apparent affinities of the various 4D5-miniantibodies to the $p185^{HER-2}$ overexpressing tumor cells SK-OV-3 were determined by radioimmunoassays, which were carried out in essentially the same manner as described previously (Willuda et al., 2001), with the following modifications. Stock solutions of the $^{99m}Tc(CO)_3$-labeled antibody constructs were prepared at 10 different concentrations by 2-fold serial dilution, and a 20-μl aliquot of each of these solutions was incubated with 100 μl of an SK-OV-3 cell suspension (corresponding to 5×10^5 cells in PBS, containing 0.5% BSA and 0.005% Tween 20) for 1 h at 4°C on a shaker. The final concentrations of active radiolabeled miniantibodies (Lindmo et al., 1984) were between 0.5 nM and 1 μM. All measurements were performed in triplicate.

Analysis of Binding Kinetics by BIAcore Measurements. The binding kinetics of the different 4D5-miniantibody formats were analyzed and compared by surface plasmon resonance measurements, using a BIAcore 3000 instrument (BIAcore AB, Uppsala, Sweden). A CM5-Sepharose chip was coated by standard amine coupling chemistry (Johnsson et al., 1991) with the recombinant extracellular domain (ECD) of the antigen $p185^{HER-2}$ to a density of 400 RU. This rather low coating density was chosen to minimize mass transfer and rebinding effects. Measurements were carried out at 25°C, using a flow rate of 30 μl/min with an association phase of 3 min after injection, followed by dissociation for 10 min. The miniantibodies were diluted in HBS-EP running buffer [10 mM HEPES, pH 7.4, 150 mm NaCl, 3 mM EDTA, 0.005% surfactant P20 (polyoxyethylene sorbitan), filtered and degassed] and injected at concentrations between 1 and 100 nM. For subtraction of bulk effects, caused by changes in the buffer composition or nonspecific binding, we performed double-referencing (Myszka, 1999). Therefore, all analyzed samples were additionally injected onto an uncoated reference surface, including a sample of the running buffer, which was also tested on the HER-2-coated flow cell. Data were evaluated with the BIAevaluation software (version 3.0), applying a simple 1:1 binding model. The obtained sensorgrams were fitted globally over the whole range of injected concentrations and simultaneously over the association and dissociation phase. Equilibrium dissociation constants were then calculated from the rate constants ($K_{D,obs} = k_{off}/k_{on}$).

Evaluation of the Immunoreactive Fraction on Cells. The percentage of immunoreactive molecules was determined by equilibrium binding assays on SK-OV-3 tumor cells, performed essentially as described by Lindmo et al. (1984). Triplicate samples with increasing numbers of cells (0.25 to 5×10^6 cells in 100 μl of PBS containing 0.5% BSA) were mixed with constant amounts of $^{99m}Tc(CO)_3$-labeled miniantibodies (in 20 μl of PBS containing 0.5% BSA and 0.005% Tween 20). The final concentration of miniantibody molecules in

these cell-suspensions was approximately 20 nM. The samples were incubated for 1 h at 4°C on a shaker. Then, cells were washed three times with PBS containing 0.5% BSA and 0.005% Tween 20, and the bound radioactivity in the cell pellets was determined by γ-scintillation counting. The obtained data were fit using a 1:1 binding model accounting for ligand depletion (see eq. A12 in Supplemental Materials with $\alpha = 0$ and $\varepsilon = 0$).

Comparison of the Association Behavior on Ni-NTA- or HER-2-Coated Surfaces. To assess the proportion of active molecules in the samples of the various miniantibody formats, we compared their association behavior on two differently coated chip surfaces in parallel by BIAcore measurements. The first was a CM5 chip, coated with the ECD of the antigen $p185^{HER-2}$ to a high density of 3700 RU; the second was an NTA chip saturated with Ni^{2+} ions. We used a slow flow rate of 5 μl/min, low analyte concentrations between 1 and 10 nM, and a short injection time of 2 min. These conditions should provide a huge excess of coated antigen over injected analyte and an association phase in which the binding of the antibody fragments on the HER-2-coated chip is mass-transport-limited and thus proportional to the amount of active molecules entering the flow cell. The Ni-NTA surface was used as a "reference cell" to determine the RU signals, according to the total amount of injected miniantibody molecules. On this surface, the constructs should be able to bind via their C-terminal His tag, whether they are denatured or in functional conformation. All measurements were performed at 25°C, using a running buffer composed of 10 mM HEPES, 150 mM NaCl, 0.005% surfactant P20, and 3 mM EDTA (HER-2 chip) or 0.05 mM EDTA (Ni-NTA chip). To evaluate the percentage of active molecules, the slopes of the sensorgrams as well as the absolute increases in response units during analyte injection determined on the HER-2 coated chip, were compared with the corresponding ones on the Ni-NTA chip.

Evaluation of the Concentration of Functional Molecules in BIAcore Measurements by Varying the Flow Rate. The concentration of functional molecules was evaluated by BIAcore analysis of the binding kinetics under partial mass transport limitation. Samples of the PEGylated and unmodified scFv 4D5 were injected at a protein concentration of 5 nM (determined by spectrophotometric measurements at 280 nm) for 2 min on a CM5 chip, coated with the ECD of $p185^{HER-2}$ to a high density of 3700 RU. Measurements were carried out at 25°C in 0.01 M HEPES, pH 7.4, 0.15 M NaCl, 3 mM EDTA, and 0.005% surfactant P20, using six different flow rates: 5, 10, 25, 50, 75, and 100 μl/min. The obtained sensorgrams were processed (subtraction of bulk effects) with the BIAevaluation software (version 3.0) and then exported into ClampXP (http://www.cores.utah.edu/interaction/clamp.html) to assess the concentration of active molecules. The sensorgrams were fitted with a 1:1 binding model under mass transport limitation:

$$L_{bulk} \underset{k_+}{\overset{k_+}{\rightleftharpoons}} L_{surface} \quad (1)$$

$$L_{surface} + R \underset{k_d}{\overset{k_a}{\rightleftharpoons}} C \quad (2)$$

Here, L_{bulk} is the analyte in the bulk phase, $L_{surface}$ is the analyte near the chip surface containing antigen linked to the dextran matrix, k_+ is the mass transport coefficient, R is the immobilized antigen (the receptor HER-2, in this case), C is the analyte-antigen complex, k_a is the intrinsic association rate constant, and k_d is the intrinsic dissociation rate constant. When the antibody fragments are injected into the flow cell, they first have to diffuse from the bulk phase to the chip surface (eq. 1), where the antigens are immobilized and the chemical binding reaction takes place. The correlation between the diffusion properties of the analyte in the sample solution and the mass transport rate is given by

$$k_+ = \frac{k_t}{h_b} \approx \frac{1}{h_b} \sqrt[3]{\frac{D_t^2 f}{0.3 h^2 w l}} \quad (3)$$

where k_+ is the transport rate constant (in seconds^{-1}), k_t is the transport velocity (in meters per second), h_b is the height of the diffusive boundary layer at the chip surface, D_t is the diffusion coefficient; f is the volumetric flow rate; and h, w, and l are the cell dimensions (height, width, and length, respectively) (BIAsimulation Software) (Christensen, 1997; Myszka et al., 1998). Fitted parameters were the intrinsic association rate constant (k_a), the intrinsic dissociation rate constant (k_d), the transport rate constant between the bulk and the surface (k_+), and the analyte concentration L_{bulk}. We used the diffusion coefficients that were independently determined by DLS. As starting points for the on- and off-rate fits, we used the k_a and k_d values that had been obtained in BIAcore measurements with a constant flow rate of 30 μl/min.

Results

In the present study, the binding properties of PEGylated monomeric scFvs and dimeric miniantibodies were characterized. To explore the effects of PEGylation on apparent affinity and related parameters, we pursued the following strategy. The PEGylation site of the antibody fragments was designed at a position as far away from the antigen binding region as possible. To ensure that the attachment of the PEG moiety did not result in a loss of functional protein, the percentage of active molecules was determined independently on tumor cells as well as in mass-transport-limited BIAcore assays. To understand the molecular basis of any effects of PEGylation on the binding properties of the antibody fragments, we analyzed the equilibrium dissociation constants, determined the on and off rates by kinetic BIAcore measurements, and evaluated the hydrodynamic sizes and diffusion coefficients by gel filtration and light scattering analyses.

Construction, Expression, and Purification of PEGylated scFv Fragments. We constructed site-specifically PEGylated variants of the scFv 4D5 and the miniantibody 4D5-dhlx (Willuda et al., 2001). The attachment site of the PEG moiety was placed in both constructs at the C terminus by introducing a single unpaired cysteine residue, separated by a glycine linker from the C-terminal His_6 tag. 4D5-dhlx contains the synthetic helix-turn-helix peptide dhlx (Hill and deGrado, 1998), which causes spontaneous dimerization of the fused proteins by self-association via hydrophobic interactions (for review, see Willuda et al., 2001). Thus, a monovalent scFv with one PEG molecule attached and a bivalent miniantibody with two PEG entities were generated (Fig. 1).

The monomeric and dimeric antibody fragments, with and without the additional cysteine residue, were all expressed in the periplasm of *Escherichia coli* SB536 and purified by two sequential affinity chromatography steps (see *Materials and Methods* and Supplemental Materials). We determined, by SDS-PAGE analysis, the purity of these proteins to be greater than 90%. For the monomeric scFv fragments and the unmodified miniantibody, we routinely obtained 2 to 3 mg/l (*E. coli* culture in shake flasks). The dimeric miniantibody with the free thiol group at the C terminus, however, yielded only approximately 500 μg/l. This reduction in yield of periplasmic proteins upon insertion of free thiols is not unexpected because of the interference with disulfide bond formation.

To prepare the antibody fragments for the PEGylation reaction, we concentrated them to approximately 0.3 to 1 mg/ml and reduced the C-terminal cysteines under mild conditions (see *Materials and Methods*) to prevent breakage of the internal disulfide bonds in the V_L and V_H domains. After removal of the reducing agent, the 20-kDa PEG polymer, containing a maleimide coupling group, was site-specifically attached to the C terminus of each antibody fragment. The conjugation yield was approximately 80 to 90%, as determined by SDS-PAGE and size exclusion chromatography (Fig. 2A). The retention of the internal disulfide bonds was verified by subjecting the unmodified scFv 4D5 to the same PEGylation procedure as described above. In this case, no attachment of the PEG polymer to the protein could be detected.

Size Exclusion Chromatography and Static Light Scattering Analysis. The apparent molecular weights of the PEGylated and unmodified antibody fragments were examined by size exclusion chromatography and static light scattering. In the gel filtration analysis, the unmodified scFv and the unmodified dimeric miniantibody eluted at a peak-volume consistent with the expected molecular weight. In contrast, their PEGylated counterparts showed retention volumes corresponding to a size in the range of 200 to 300 kDa, whereas the molecular mass is only 50 kDa for the monomer-PEG20 and 100 kDa for the dimer-PEG20 (Fig. 2A). This result is in agreement with the findings of other groups (Chapman, 2002; Greenwald et al., 2003; Harris and Chess, 2003; Yang et al., 2003). It demonstrates the strong effect of the 20-kDa PEG tail on the hydrodynamic properties of the conjugated protein, enlarging its hydrodynamic radius far beyond that expected for the given increase in molecular mass.

Static light scattering, which was performed online during gel filtration runs, confirmed the calculated molecular weights of the different constructs, rather than the apparent hydrodynamic sizes. Thus, it could be shown that the desired molecular species had indeed been prepared. We determined a size of 29.7 kDa for the scFv 4D5 (predicted, 29.2 kDa), 63.5 kDa for the dimer 4D5-dhlx-SS (predicted, 66.5 kDa), and 61 kDa for the PEGylated monomer 4D5-PEG20 (predicted, 50 kDa) (Fig. 2B). Only the mass of the PEGylated dimer 4D5-dhlx-PEG20 could not be determined reliably, because it eluted at a volume close to the exclusion volume of the Superdex 200 column, where it overlapped with a scatter peak caused by abrasion of the injection valve.

Determination of Diffusion Coefficients by Dynamic Light Scattering Analysis. Size exclusion chromatography analysis indicated that the 20-kDa PEG tail has a strong effect on the hydrodynamic volume of the attached proteins. To verify this conclusion and exclude any interference of the column material, we examined and compared the translational diffusion of the PEGylated and unmodified antibody fragments in solution by DLS. Measurements were performed with protein concentrations between 650 μg/ml and 1.3 mg/ml. For data evaluation, we used a monomodal size distribution model and, for each set of data, determined a translational diffusion coefficient representing the mean fraction of scatter and mass percentage.

We assessed a diffusion coefficient (D_t) of 8.4×10^{-7} cm^2/s for the monomeric scFv 4D5 and 6.0×10^{-7} cm^2/s for the dimer 4D5-dhlx. For each PEGylated construct, two mean scatter peaks were detected, corresponding to D_t values of 3.1 and 4.4×10^{-7} cm^2/s (Table 1). For the PEGylated scFv 4D5-PEG20, 70% of the data corresponded to a D_t value of 4.4×10^{-7} cm^2/s, whereas for the PEGylated dimer 4D5-dhlx-PEG20 only 35% corresponded to this value. The majority of the data (50%) for this PEGylated dimer corresponded to a D_t value of 3.1×10^{-7} cm^2/s. Comparing the PEGylated species with their unmodified counterparts, it seems that PEGylation decreased the diffusion coefficient of the antibody fragments by approximately 2-fold. Based on these values, we calculated the apparent molecular weights of the constructs when treated as globular proteins. For the unconjugated scFv fragments, we determined sizes of 27 kDa (monomeric scFv 4D5) and 61 kDa (dimeric miniantibody 4D5-dhlx), which are consistent with the predicted molecular weights. The diffusion coefficients of these PEGylated constructs, however, correspond to sizes of 133 and 309 kDa, respectively. These values are clearly above their actual molecular mass and completely consistent with the findings of the gel filtration analysis. Most important for the evaluation of the binding properties was the observation that PEGylation did decrease the diffusion coefficients of the antibody fragments, as expected, but only by approximately 2-fold.

Comparison of Binding Kinetics by Surface Plasmon Resonance. The apparent affinities of the 4D5-derived antibody fragments to their target antigen $p185^{HER-2}$ were examined by radioimmunoassays on SK-OV-3 tumor cells and by BIAcore measurements. We found a 5-fold decrease in apparent affinity upon attachment of the 20-kDa PEG moiety for both the monomeric and the dimeric antibody fragment (Table 2). As explained in the subsequent section, we can exclude a difference in the percentage of functional molecules as a possible cause.

To investigate this observation in more detail, we compared the binding kinetics of the different constructs by separate analysis of the association and dissociation rates using surface plasmon resonance (Fig. 3). The antigen was coated on a CM5 chip at a relatively low density of 400 RU, and measurements were performed at a high flow rate of 30 μl/min. This setup was chosen to minimize mass transport effects and rebinding of fully dissociated molecules, which both could compromise the measured kinetics. The determined k_{on}, k_{off}, and $K_{D,obs}$ values are given in Table 3 and reveal that the reduction in functional affinity, caused by PEGylation of the antibody fragments, is due almost exclusively to a slower on rate, whereas the off rate is nearly unchanged. The PEGylated scFv 4D5-PEG20, for example, showed a k_{on} of 6.1×10^4 M^{-1} s^{-1}, which is approximately 5.5-fold smaller than that of the corresponding scFv 4D5, displaying a k_{on} of 3.4×10^5 M^{-1} s^{-1}. However, their dissociation rates, determined as 4.9×10^{-5} s^{-1} (4D5-PEG20) and 5.0×10^{-5} s^{-1} (scFv 4D5), are virtually the same. While this work was in progress, similar findings were also reported for other scFv fragments that had been site-specifically conjugated with PEG polymers of different sizes (Yang et al., 2003). When comparing the binding kinetics of these constructs with the corresponding binding kinetics of the un-PEGylated scFvs, a modest effect was found if a small PEG molecule of 5 kDa was attached, whereas conjugates modified with a 20- or 40-kDa PEG tail displayed a reduction in on rate of as much as 100-fold. Consistent with our data, the

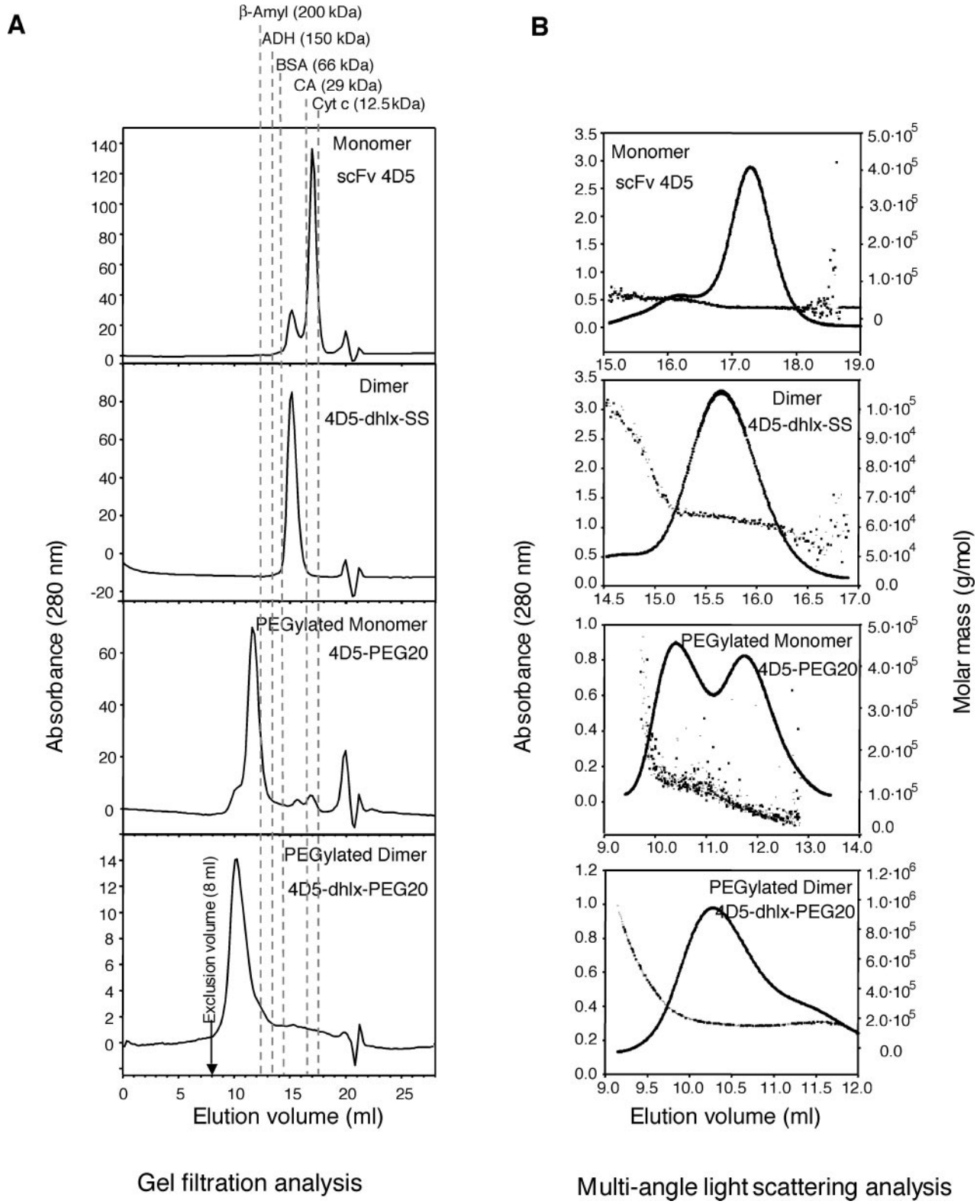

Fig. 2. Analysis of the size and format of the PEGylated and unPEGylated antibody fragments. The apparent hydrodynamic sizes and the actual molecular masses of the scFv 4D5 (theoretical, 29 kDa), the dimeric miniantibody 4D5-dhlx-SS (theoretical, 66 kDa), the PEGylated scFv 4D5-PEG20 (theoretical, 50 kDa), and the PEGylated dimeric miniantibody 4D5-dhlx-PEG20 (theoretical, 106 kDa) were investigated by gel filtration analysis (A) and static light scattering analysis (B). A, gel filtration analysis was carried out on an ÄKTAexplorer system with a Superdex-200 column (24-ml bed-volume). For calibration, the following molecular mass standards were used and their elution volumes are shown with vertical dashed lines: β-amylase (200 kDa), alcohol dehydrogenase (150 kDa), bovine serum albumin (66 kDa), carbonic anhydrase (29 kDa), and cytochrome *c* (12.5 kDa). The elution volumes of the antibody fragments were 17.0 ml (scFv 4D5), 15.09 ml (4D5-dhlx-SS), 13.03 ml (4D5-p53-SS), 11.88 ml (4D5-PEG20), and 10.15 ml (4D5-dhlx-PEG20). B, dynamic light scattering analysis was performed with the tri-angle light scattering detector miniDAWN (Wyatt) in combination with the interferometric refractometer OPTILAB (Wyatt), which were both serially connected to the ÄKTAexplorer size exclusion chromatography system. We assessed molecular masses of 29.7 kDa for the scFv 4D5, 63.5 kDa for the dimeric miniantibody 4D5-dhlx-SS, and 61 kDa for the PEGylated scFv 4D5-PEG20. The molecular mass of the PEGylated dimeric miniantibody 4D5-dhlx-PEG20 could not be determined.

dissociation rates of these conjugates were nearly equivalent to those of the unmodified scFvs.

To better understand the molecular mechanism(s) by which the observed association rates of the PEGylated analogs are reduced, we experimentally tested and computationally simulated several possible hypotheses (Fig. 4).

Evaluation of the Fraction of Functional Molecules. These experiments test the hypothesis depicted in Fig. 4A. During PEGylation, the antibody fragments were first incubated with 3 mM dithiothreitol at 37°C for 30 min and, after removal of this reducing agent, they were further incubated at 37°C for 2 h with maleimide-PEG20. Although the results of previous stability analyses (S. Kubetzko, E. Balic, R. Waibel, U. Zangemeister-Wittke, and A. Plückthun, manuscript in preparation; for review, see Willuda et al., 2001) indicate that the 4D5-derived antibody fragments are stable under these conditions, it was essential to directly determine the fraction of functional proteins. For this purpose, the binding activity of the PEGylated and unmodified antibody fragments was analyzed on whole cells as well as by BIAcore measurements.

We assessed their immunoreactivity on human SK-OV-3 tumor cells by applying the method described by Lindmo et al. (1984), where an increasing number of cells were used to saturate all antibody molecules with antigen. We determined the percentage of active molecules to be approximately 85 to 94% for all constructs, without observing a significant difference caused by PEGylation of the antibody fragments (Table 4).

In addition, we examined the binding reactivity of the 4D5-miniantibodies by surface plasmon resonance measurements on a BIAcore 3000 instrument under mass-transport limitation, using two different approaches. First, we compared their association behavior on two different chips in parallel (Fig. 5). One was a CM5 chip, coated to a high density (3700 RU) with the target antigen, the ECD of HER-2, and the other was a Ni-NTA chip. The HER-2-coated chip surface served as the "measuring cell" to determine the fraction of active molecules in the injected protein samples that is capable of antigen binding. The Ni-NTA chip was used as the "reference cell" to estimate the RU values corresponding to 100% of the molecules present. On this nickel-saturated surface, the antibody fragments should be able to associate via their C-terminal His tags, whether they are denatured or in an active conformation. In all measurements, a slow flow rate (5 μl/min), low analyte concentrations (1–10 nM), and a short injection time (2 min) were used. By employing these conditions we wanted to approach the situation where analyte binding is mass-transport-limited and thus proportional to the concentration of active molecules, resulting in linear association slopes. In accordance with the data of the cell-binding assays, we determined a fraction of 90 to 100% active molecules for all constructs.

In the second set of BIAcore analyses, we used a method that relies on the change in binding rate with varying flow rate at a high concentration of coated antigen (Richalet-Sécordel et al., 1997). When the density of immobilized antigen is very high, the mass transport of the analyte from the bulk solution to the chip surface becomes partially rate limiting, which can be observed by an increase in binding rate with increasing flow rate at constant analyte concentration (Myszka et al., 1998). This effect can be exploited to determine the active concentration of the injected protein sample, because the association rate under mass transfer limitation is proportional to the concentration of active molecules. We compared the binding kinetics of the PEGylated and the unmodified scFv 4D5 at different flow rates between 5 and 100 μl/min, both injected at a protein concentration of

TABLE 1

Dynamic light scattering analysis of the translational diffusion coefficient (D_t) and hydrodynamic size

Measurements were carried out with the one-angle (90°) DLS-instrument DynaPro. Data were evaluated with the software DYNAMICS version 4.0, using a monomodal size distribution model. Constructs are described in Fig. 1.

Construct	D_t	R_h	Molecular Mass for Spherical Protein
	cm^2/s	nm	kDa
Monomer: scFv 4D5	8.4×10^{-7}	2.5	27
Dimer: 4D5-dhlx-SS	6.0×10^{-7}	3.5	61
PEGylated-monomer:	4.4×10^{-7} (70%)	4.8	133
4D5-PEG20	3.1×10^{-7} (22%)	6.8	309
PEGylated dimer:	4.4×10^{-7} (35%)	4.8	133
4D5-dhlx-PEG20	3.1×10^{-7} (50%)	6.8	309

R_h, hydrodynamic radius, based on the determined diffusion coefficient.

TABLE 2

Functional affinity of the 4D5-derived antibody fragments on SK-OV-3 tumor cells

Binding interaction of the ^{99m}Tc-labeled antibody fragments with the p185^{HER-2}-overexpressing tumor cells SK-OV-3 was measured in a RIA format at 4°C (see *Materials and Methods*). Apparent affinities were calculated from the fit of the data, using the simplified equation $C = R_{0,obs}L/(K_{D,obs} + L)$. We thus assumed a simple 1:1 binding model, even though only the monomeric antibody fragments are properly described by this model.

Antibody Fragment	Functional Affinity on SK-OV-3 Cells
	nM
Monomer: scFv 4D5	29.3 ± 5.2
Dimer: 4D5-dhlx-SS	11.9 ± 1.0
PEGylated monomer: 4D5-PEG20	138 ± 37
PEGylated dimer: 4D5-dhlx-PEG20	67 ± 7

TABLE 3

Binding kinetics of the PEGylated and unPEGylated molecules

Presented values refer to the kinetic BIAcore measurements in Fig. 3. The S.E. for each k_{on} value is less than 1%; that for each k_{off} value is less than 11%. These data are representative of at least two independent experiments for each construct, and S.E. for all experiments is less than 12%. We expect that additional errors in the concentrations of active species will contribute another 15% (see Table 4).

Construct	k_{on}	k_{off}	$K_{D,obs}$	χ^2
	$M^{-1}\ s^{-1}$	s^{-1}	M	
Monomer	3.4×10^5	5.0×10^{-5}	1.5×10^{-10}	0.7
Monomer-PEG20	6.1×10^4	4.9×10^{-5}	8.1×10^{-10}	0.6
Dimer	9.8×10^5	2.6×10^{-5}	2.6×10^{-11}	4.2
Dimer-PEG20	2.7×10^5	3.5×10^{-5}	1.3×10^{-10}	1.9

TABLE 4

Immunoreactivity of the PEGylated and unPEGylated anti-p185^{HER-2} antibody fragments on human SK-OV-3 tumor cells

The antibody fragments were radioactively labeled with ^{99m}Tc(CO)$_3$ and the percentage of active molecules was determined for each construct by equilibrium binding assays on SK-OV-3 cells as described by Lindmo et al. (1984). The data were fit using a 1:1 binding model accounting for ligand depletion (see eq. A12 in Supplemental Materials with $\alpha = 0$ and $\varepsilon = 0$). Immunoreactive fraction means binding to the p185^{HER-2} antigen with at least one binding site.

Antibody Fragment	Immunoreactive Fraction on Cells
	%
Monomer: scFv 4D5	94
Dimer: 4D5-dhlx-SS	89
PEGylated monomer: 4D5-PEG20	90
PEGylated dimer: 4D5-dhlx-PEG20	85

5 nM (Fig. 6). Again, the evaluated percentage of active molecules of the PEGylated construct did not deviate markedly from that of the unconjugated scFv. We thus conclude that the percentage of functional proteins is very similar for all constructs and is at least 85%.

Effect of Diffusion on Observed Binding Kinetics. We now consider the hypothesis depicted in Fig. 4B. Having measured approximately a 2-fold decrease in the translational diffusion coefficients for the PEGylated constructs by DLS, we wanted to determine what effect this might have on the observed binding kinetics. Therefore, a mathematical model was formulated to gain more insight into the effect of translational or rotational diffusion on the observed binding kinetics. The model involves translational or rotational transport of the bulk ligand (L, molar) (in our case, the antibody) to a binding-competent state at the surface (L_s, molar). This binding-competent ligand can then either bind reversibly to an immobilized receptor (R, in moles/area) (in our case, the antigen) to form a complex (C, in moles/area) or be transported back to the bulk

$$L \underset{k_+}{\overset{k_+}{\rightleftharpoons}} L_s; \quad L_s + R \underset{k_d}{\overset{k_a}{\rightleftharpoons}} C \tag{4}$$

where k_+ is the transport rate constant (in seconds^{-1}) that depends on the respective diffusion coefficient and the geometry of the system (e.g., eqs. 3 and A8 in Supplemental Materials) (Lauffenburger and Linderman, 1993). Note, however, that the basic mathematical formulation is identical for translational and rotational diffusion, and for the purposes of this analysis, we do not need to consider the explicit form of k_+. The intrinsic association and dissociation rate constants are k_a (in molar^{-1} seconds^{-1}) and k_d (in seconds^{-1}), respectively. When the concentration of the intermediate L_s is small and this species is short-lived, we can invoke the pseudo–steady-state approximation:

$$\frac{dL_s}{dt} = k_+ L - k_+ L_s + \frac{1}{h_b}(k_d C - k_a L_s R) \approx 0$$

$$\Rightarrow L_s = \frac{k_t L + k_d C}{k_t + k_a R} \tag{5}$$

where h_b is the height of the diffusive boundary layer at the surface, and the transport velocity $k_t = h_b k_+$ (in meters per second). The rate of change in complexes is given by

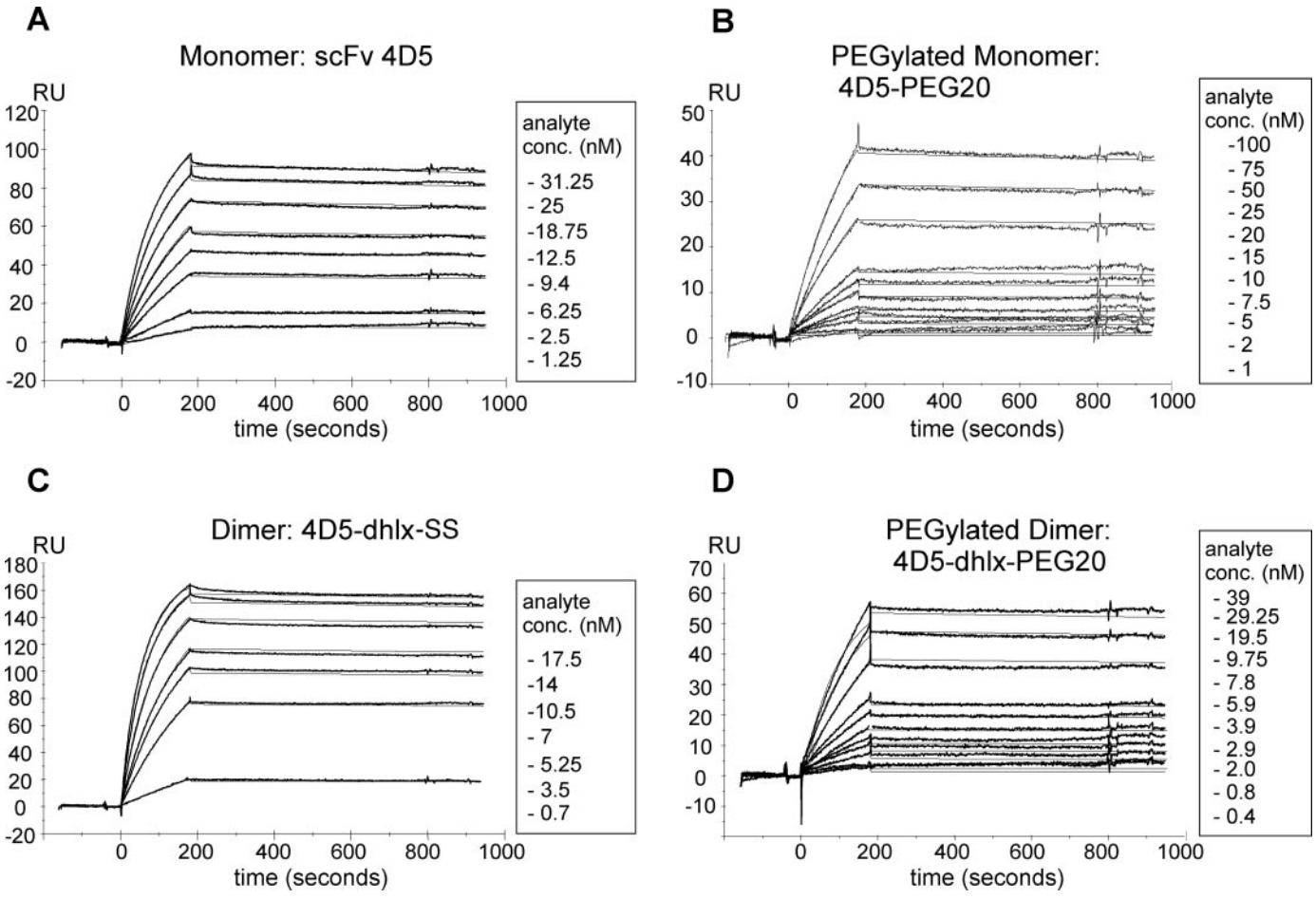

Fig. 3. Comparison of the binding kinetics of the PEGylated and unPEGylated antibody fragments by BIAcore measurements. Association and dissociation kinetics of the monomeric scFv 4D5 (A), the PEGylated scFv 4D5-PEG20 (B), the dimeric miniantibody 4D5-dhlx (C), and the PEGylated dimeric miniantibody 4D5-dhlx-PEG20 (D) were compared by surface plasmon resonance measurements, using a BIAcore 3000 instrument. A CM5-Sepharose chip (BIAcore AB) was coated with p185^{HER-2}-ECD antigen to a density of 400 RU. The constructs were injected at a high flow rate of 30 μl/min, using concentrations between 1 and 100 nM. Associations were monitored for 3 min and dissociations for 10 min. Data were evaluated with the BIAevaluation 3.0 software (BIAcore AB), applying a simple 1:1 binding model and a global fit. An overlay of experimental data and global curve fits is shown.

$$\frac{dC}{dt} = k_a L_s R - k_d C = k_{on} L R - k_{off} C \quad (6)$$

In eq. 6, the first equality gives the rate of change in terms of the intrinsic rate constants and L_s, whereas the second equality gives it in terms of the experimentally measured quantities k_{on} (in molar^{-1} seconds^{-1}), k_{off} (in seconds^{-1}), and L. Plugging the result for L_s from eq. 5 into the first equality in eq. 6 gives

$$\frac{dC}{dt} = \left(\frac{k_t k_a}{k_t + k_a R}\right) L R - \left(\frac{k_t k_d}{k_t + k_a R}\right) C \quad (7)$$

Direct comparison of the second equality in eq. 6 with eq. 7 reveals:

$$k_{on} = \left(\frac{k_t}{k_t + k_a R}\right) k_a \quad \text{and} \quad k_{off} = \left(\frac{k_t}{k_t + k_a R}\right) k_d$$

$$\Rightarrow \frac{k_{off}}{k_{on}} = \frac{k_d}{k_a} \quad (8)$$

In other words, transport limitations that occur when k_t is not far greater than $k_a R$ would reduce the apparent association and dissociation rate constants by the same percentage, thus giving an apparent equilibrium dissociation constant $K_{D,obs}$ ($= k_{off}/k_{on}$) identical to the intrinsic K_D ($= k_d/k_a$). This is not consistent with the experimental data, because only the observed association rate constant is reduced, resulting in a 5-fold higher $K_{D,obs}$ (5-fold lower affinity). In addition, the BIAcore data for each PEGylated molecule were fit with both a simple 1:1 binding model and the model accounting for mass-transport limitations (see *Materials and Methods*), and both models gave the same values for k_{on} and k_{off} for a given molecule. This suggests that, in our BIAcore experimental setup, $k_t \gg k_a R$; therefore, we can rule out the effect of any diffusion limitations in our kinetic measurements.

For translational diffusion limitations on cells, it can be shown that $k_t = D_t/r_c$ (Smoluchowski, 1917), where D_t is the translational diffusion coefficient and r_c is the radius of the cell (see Supplemental Materials). In this case, we can see from eq. 8 that

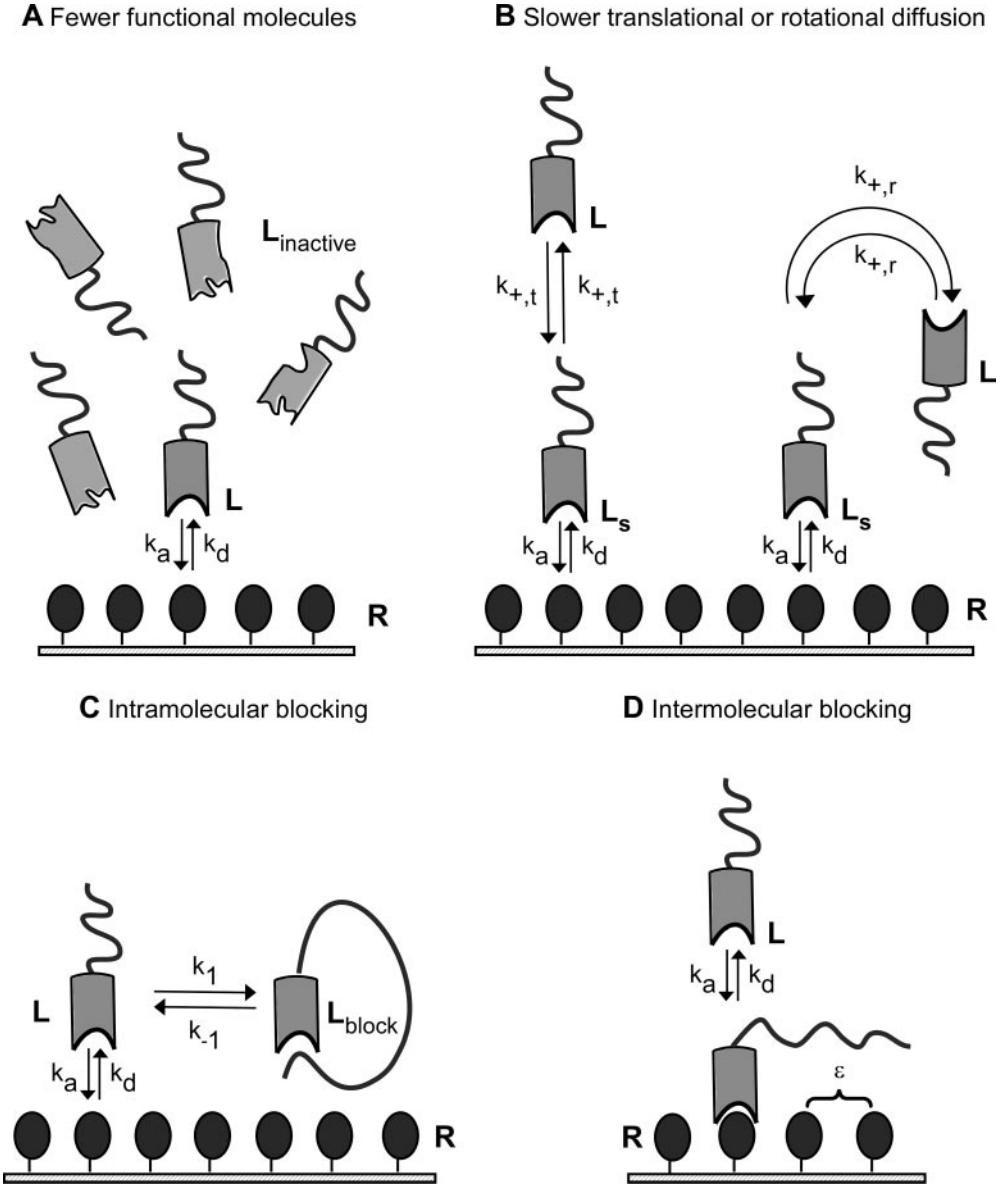

Fig. 4. Diagram presenting potential reasons for the decrease in apparent on rates of the PEGylated molecules. There are several factors that could, in principle, lead to reduced on rates upon PEGylation of antibody fragments. A, the presence of permanently inactive molecules ($L_{inactive}$) would result in a lower percentage of functional molecules (L) that are capable of binding reversibly to immobilized receptor (R) with forward and reverse rate constants k_a and k_d, respectively. B, a translational or rotational diffusion limitation (resulting from reduced transport rate constant $k_{+,t}$ or $k_{+,r}$, respectively) would slow the delivery of bulk ligand (L) both to and from the surface. Surface-proximal ligand (L_s) could bind reversibly to R with forward and reverse rate constants k_a and k_d, respectively. C, the PEG moiety could intramolecularly block the binding region of the antibody, with rate constant k_1, to form L_{block}. Unblocked ligand (L) could be regenerated from L_{block} with unblocking rate constant k_{-1}. L could bind reversibly to R with forward and reverse rate constants k_a and k_d, respectively. D, L could bind reversibly to R with forward and reverse rate constants k_a and k_d, respectively. However, in the bound state, the PEG tail could hinder antibody binding to ε adjacent sites through intermolecular blocking; thus, a single PEGylated antibody would occupy $(1 + \varepsilon)$ sites on the surface.

$$\frac{k_{on}}{k_a} = \frac{k_{off}}{k_d} = \frac{1}{1 + Da}; \quad Da = \frac{k_a R}{D_t / r_c} \tag{9}$$

where Da is the Damköhler number, quantifying the ratio of the reaction (binding) velocity to the transport (diffusion) velocity. When diffusion is very fast compared with binding, then $Da \ll 1$ and the intrinsic kinetics are observed experimentally. The particular form of this solution is simply a specialized case of the general result described above (eq. 8). Thus, the observed K_D on cells should also be unaffected by diffusion limitations. Because the PEGylated species have lower equilibrium affinities than their unPEGylated counterparts (Table 3), this suggests that mechanisms other than slower diffusion contribute to the binding of the PEGylated molecules.

This model with spherical cells was used to simulate the binding kinetics that may be observed on cells expressing 20,000 and 2,000,000 receptors (Fig. 7). For HER-2, these values roughly correspond to the expression levels seen in normal breast tissue and in breast cancer cells, respectively. On normal cells (Fig. 7, A and B), diffusion limitations in observed binding kinetics become significant only at very high k_a values ($>10^7$ M^{-1} s^{-1}) for ligands with D_t values similar to those in the current study (10^{-7} to 10^{-6} cm^2/s; Table 1). However, various experimental studies summarized by Northrup and Erickson (1992) (and further analyzed computationally by these authors) suggest that the intrinsic association rate constant for protein-protein interactions in normal salt conditions does not normally exceed 5×10^6 M^{-1} s^{-1}. On the other hand, in tumor cells with high receptor numbers, k_aR increases Da significantly, and thus the observed kinetics are slowed compared with intrinsic kinetics (Fig. 7, C and D). These numbers particularly apply to ligands with properties similar to those of the dimer and dimer-PEG species in the current study. Thus, in the absence of rapid internalization or degradation processes, the ligands are predicted to have longer mean residence times on the surfaces of cancer cells than on those of normal cells, which may be a desirable effect for sustained, localized delivery of radionuclides or other agents to cancer cells. The decrease in the observed association rate constant compared with the intrinsic one can be rationalized as an increase in competition, under slow delivery of ligand, for binding of each receptor by neighboring receptors; likewise, the decrease in the observed dissociation rate constant can be linked to greater rebinding effects at higher receptor densities relative to diffusion of ligand away from the surface.

Effect of Intramolecular and Intermolecular Blocking on Observed Binding Kinetics and Equilibrium Affinities. We finally explore the hypotheses depicted in Fig. 4, C and D. Although the PEG moiety was chemically linked to a position as far as possible from the antigen binding site, it is still possible that the flexible polymer sterically blocks the binding interface. Based on the hydrodynamic radius of the monomeric scFv (see Table 1), its half-circumference is ~7.8 nm. The Flory radius ($R_F \sim aN^{0.6}$) of a PEG molecule with a molecular mass of 20 kDa (a = 0.35 nm, length of a monomer; $N \approx 450$ units) is ~14 nm in aqueous solution; in fact, previous work with PEG tethers suggests that the average end position may lie even further ($R_e \sim aN^{0.64}$) from the attachment point (Jeppesen et al., 2001). Regardless, the PEG would sample conformations up to its fully extended length, which would be ~160 nm for a 20-kDa moiety. Based on these length scales, the polymer chain could easily access the site of the protein most distal to its attachment point. Thus, one possibility is that the PEG moiety

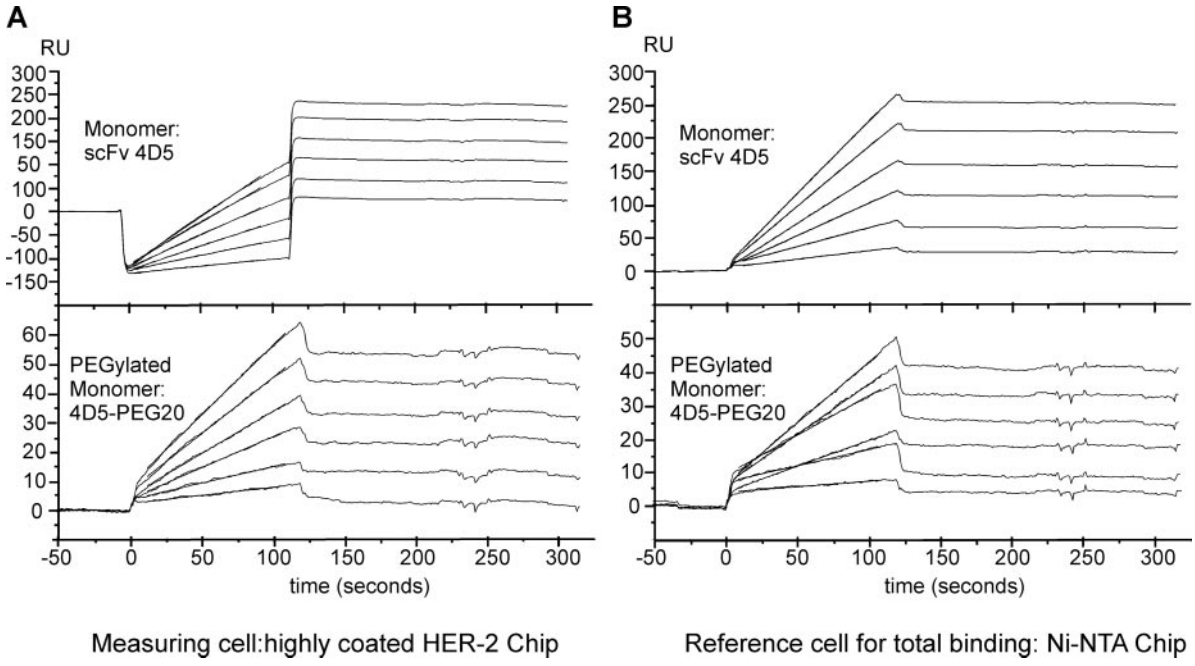

Fig. 5. Comparison of binding rates on a HER-2-coated surface and a Ni-NTA-coated surface by BIAcore measurements to assess the percentage of active molecules. Samples of the various miniantibody formats were injected onto a CM5 chip, containing HER-2 antigen at a high density (3700 RU) (A), and onto an NTA chip, saturated with Ni^{2+} ions (B). A slow flow rate of 5 μl/min, low analyte concentrations between 1 and 10 nM, and a short injection time of 2 min were used. The proportion of functional molecules was evaluated by comparison of the association rates on the HER-2-coated chip with the corresponding ones on the Ni-NTA chip. Here, only the sensorgrams of the unmodified scFv 4D5 and the PEGylated monomeric scFv 4D5-PEG20 are shown.

acts intramolecularly to dynamically block the antigen-binding site on the antibody itself (Fig. 4C).

Another major consequence of PEGylation is that it greatly increases the effective size of the molecule. As far as total collisions are concerned, they would be expected to be independent of size in the spherical approximation, because the larger radius of the protein increases the target size but also reduces diffusivity, such that these two effects exactly cancel (Smoluchowski, 1917; Janin, 1997). The fraction of successful collisions among all collisions, however, is proportional to the fraction of surface area comprising the binding site (Janin, 1997), and thus the observed association rate constant should decrease if the area of the binding site is held constant but the total surface area of the ligand is increased by PEGylation. PEGylation may also indirectly affect the binding properties of the ligand via interactions that change the plasticity or surface charge distribution of the molecule (Kerwin et al., 2002). Here, we use the term 'intramolecular blocking' to encompass all of these indistinguishable effects that the PEG moiety may have on the molecule to which it is coupled.

A second possibility is that, once a PEGylated antibody molecule binds to its antigen on a surface, the polymer tail acts intermolecularly to hinder binding of antibodies to adjacent antigen molecules (Fig. 4D). This is analogous to the 'parking problem' in adsorption kinetics (Evans, 1993; O'Shannessy and Winzor, 1996). This latter mechanism is also plausible, because the average distance between receptor molecules, assuming uniform receptor density, was calculated to be in the range of 20 to 30 nm in both the BIAcore setup and on the SK-OV-3 cells used in our experiments; in reality, it is likely that the receptors are clustered, thereby reducing this intermolecular spacing.

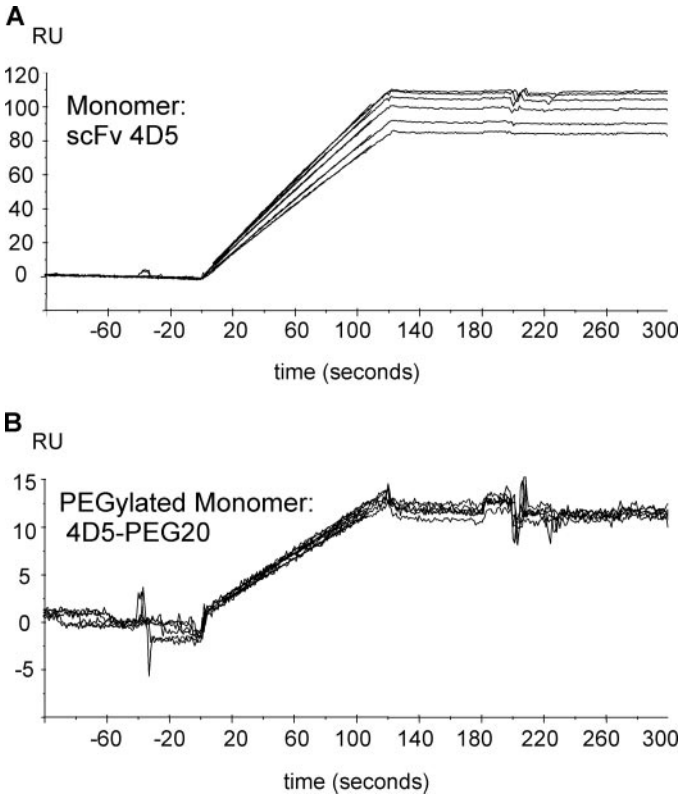

Fig. 6. Evaluation of the concentration of functional molecules by BIAcore measurements with varied flow rates. The binding kinetics of the scFv 4D5 (A) and its PEGylated counterpart 4D5-PEG20 (B) were analyzed under partial mass transport limitation. Low concentrated samples (approximately 5 nM) of the constructs were injected onto a CM5 chip densely coated with the antigen HER-2 (3700 RU). Association was followed for 2 min at six different flow rates (5, 10, 25, 50, 75, and 100 μl/min). Sensorgrams were exported into ClampXP (http://www.cores.utah.edu/interaction/clamp.html) and data were evaluated by applying a 1:1 binding model under mass transport limitation (see text, eqs. 1 and 2), setting the analyte concentration as parameter to fit.

If these two blocking modes are the only major factors affecting the binding kinetics, the relevant processes are:

$$L \underset{k_{-1}}{\overset{k_1}{\rightleftharpoons}} L_{\text{block}}; \quad \alpha = \frac{k_1}{k_{-1}}$$

$$L + R \underset{k_d}{\overset{k_a}{\rightleftharpoons}} C; \; K_D = \frac{k_d}{k_a}; \; R_0 = R + (1+\varepsilon)C \tag{10}$$

The parameter α describes the degree of intramolecular blocking of ligand L to give blocked ligand L_{block} (Fig. 4C) and is equal to the equilibrium constant between the unblocked and blocked states of the ligand. Free receptors (R) can be bound by L to give complexes (C). The parameter ε describes the degree of intermolecular blocking and is equal to the effective number of additional receptors sterically blocked by a bound ligand (Fig. 4D). Thus, the total number of receptors (R_0) is the sum of unbound, accessible receptors (R), bound receptors (C), and unbound receptors blocked by bound receptors (εC). It should be noted that α is an intrinsic property of the ligand and thus independent of the experimental setup; however, ε may depend on the receptor density or clustering.

In BIAcore, there is a continuous flow of fresh buffer, so it is reasonable to assume that the concentrations of ligand (L and L_{block}) in the flow cell do not change appreciably from those in the buffer entering the flow cell. Thus, the total ligand concentration in the flow cell is:

$$L_0 = L + L_{\text{block}} = L(1+\alpha) \tag{11}$$

The change in complexes with respect to time can be described using mass-action kinetics:

$$\frac{dC}{dt} = k_a LR - k_d C = k_a\left(\frac{L_0}{1+\alpha}\right)(R_0 - (1+\varepsilon)C) - k_d C \tag{12}$$

Solving this result for the association phase [$C(0) = 0$] (see Supplemental Materials) and arranging terms:

$$C = \frac{R_0}{1+\varepsilon} \times \frac{L_0}{L_0 + \left(\frac{1+\alpha}{1+\varepsilon}\right)K_D} \times \left(1 - e^{-\left(\left(\frac{1+\varepsilon}{1+\alpha}k_a\right)L_0 + k_d\right)t}\right) \tag{13}$$

From eq. 13, it is clear that intramolecular blocking ($\alpha > 0$) can reduce the apparent association rate constant [$k_{on} = (1+\varepsilon)k_a/(1+\alpha)$] and increase the apparent equilibrium dissociation constant [$K_{D,obs} = (1+\alpha)K_D/(1+\varepsilon)$], because k_{off} would be unaffected. Conversely, intermolecular blocking ($\varepsilon > 0$) has the opposite effect on both of these parameters and, furthermore, decreases the apparent number of binding

sites [$R_{0,obs} = R_0/(1 + \varepsilon)$]. The counterintuitive result of having a higher k_{on} and a lower $K_{D,obs}$ as a result of intermolecular blocking is explained later in this section.

The result in eq. 13 is simulated in Fig. 8A for different values of α and ε. Here, it can be seen that the initial rate of binding is dependent on α, but actually independent of ε. When very few antigens are bound, there is not a pronounced effect of intermolecular blockage; consequently, intramolecular blockage limits the rate of association. Because the number of ligand-receptor complexes at the beginning of any time course is zero, we can evaluate eq. 12 at $C(0) = 0$ to obtain a mathematical expression for the initial rate of change in complexes:

$$\frac{dC}{dt}(t = 0) = \left(\frac{1}{1 + \alpha}\right) k_a L_0 R_0 = \left(\frac{1 + \varepsilon}{1 + \alpha} k_a\right) L_0 \frac{R_0}{1 + \varepsilon}$$

$$= k_{on} L_0 R_{0,obs} \quad (14)$$

Note that this expression is indeed independent of ε (because of the cancellation of its effect on k_{on} and $R_{0,obs}$ at $t = 0$) and

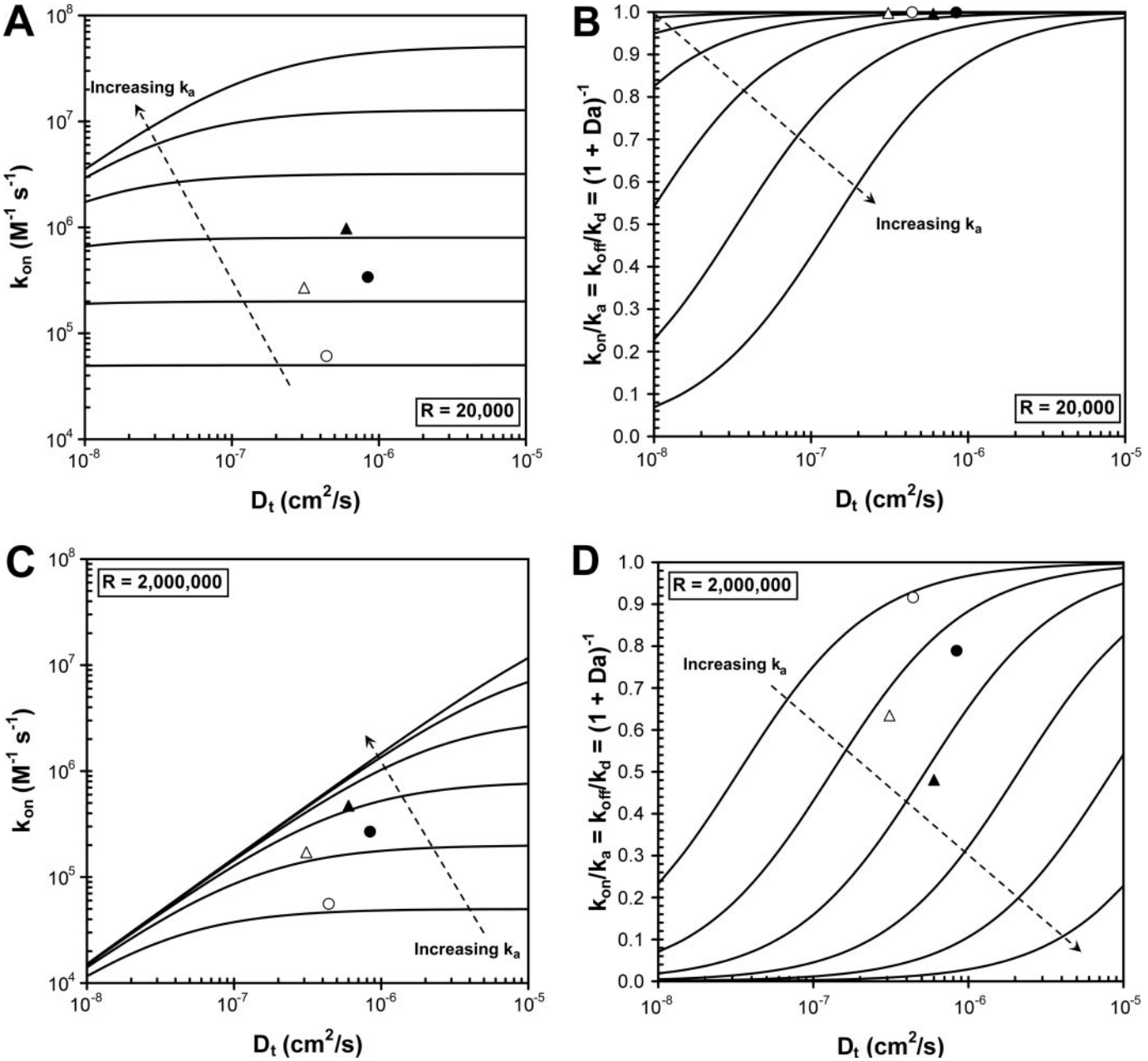

Fig. 7. Mathematical model of the influence of translational diffusion coefficient, intrinsic association rate constant, and receptor overexpression on observed binding kinetics. A, observed association rate constant (k_{on}) as a function of translational diffusion coefficient (D_t) and intrinsic association rate constant (k_a) at a receptor expression level of 20,000 per cell, which, for HER-2, is comparable with that seen in normal human breast tissue. For units of moles/area, $R = 20{,}000/(4\pi r_c^2 N_A)$, where r_c is the cell radius (10 μm) and N_A is Avogadro's number. The values of k_a in the simulation are multiples of 4 from $5 \times 10^4\ M^{-1}\ s^{-1}$ to $5.12 \times 10^7\ M^{-1}\ s^{-1}$. B, observable rate constants [as fraction of intrinsic (maximal) kinetic rate constants (k_{on}/k_a and k_{off}/k_d)] as a function of D_t and k_{on}. The Damköhler number ($D\alpha$), equal to $k_a R/(D_t/r_c)$, gives the ratio of the binding velocity to the diffusion velocity. C and D, similar to A and B, respectively. Here, however, the receptor number is 2,000,000 per cell, which, for HER-2, is comparable with the overexpression level found in human breast cancer cells. Symbols represent the predicted behaviors of the scFv (●), scFv-PEG (○), dimer (▲), and dimer-PEG (△) from this study, based on their experimentally measured D_t values.

corresponds to the initial, linear portion of an association binding curve. At intermediate times, both types of blockage significantly affect the binding profile in Fig. 8A. As the binding reaction reaches equilibrium ($t \rightarrow \infty$ in eq. 13), the value of C_{eq}, the equilibrium number of complexes formed, also depends on both α and ε. However, if $L_0 \gg (1 + \alpha)K_D/(1 + \varepsilon)$:

$$C_{eq} \approx \frac{R_0}{1 + \varepsilon} \quad (15)$$

It should be noted that the dissociation phase ($L_0 = 0$ in eq. 12) is unaffected by either blocking mechanism.

With eqs. 14 and 15, we have independent methods for estimating α and ε, respectively. The simplest way to test experimentally whether intermolecular blocking influences the kinetics in BIAcore is to perform measurements at very high ligand concentrations and allow the flow cell to reach equilibrium. After proper referencing, the observed signal $RU_{max} = (mR_o)(MW)/(1 + \varepsilon)$, where m is a proportionality constant and MW is the molecular weight of the ligand. For an unmodified antibody, $\varepsilon = 0$; therefore, RU_{max} is directly proportional to $(R_0)(MW)$. Performing the same analysis with the PEGylated analog should directly yield ε. To determine whether this blocking is significant for our PEGylated constructs, both unmodified and PEGylated monomer were passed, at very high concentrations (~1 μM), over an antigen-coated BIAcore chip—importantly, the same chip used for the kinetic analyses because coating density affects ε—and RU_{max}/MW values were determined. For the PEGylated monomer, this value was approximately three times smaller than that for the unmodified monomer (Table 5), which corresponds to an ε value of approximately 2. This suggests that the PEG chain of each bound scFv fragment can hinder the association of additional scFv-PEG molecules to approximately two neighboring antigens, as spaced in this experiment.

We have determined experimentally that the observed association rate of the PEGylated monomer is ~5.4-fold slower than that of the unmodified monomer, and this corresponds directly to a 5.4-fold decrease in equilibrium affinity. For the model to capture this observation [i.e., $(1 + \alpha)/(1 + \varepsilon) = 5.4$], the value of α must be ~15.

Is the experimentally measured ratio of initial association rates smaller than the k_{on} ratio, as predicted by the model? And, if so, does the value of α obtained from the experimental $K_{D,obs}$ values match well with the α calculated from the initial association rates? From Table 5, we see that the answer to both of these questions is yes. It should be noted that, a priori, the experimental $K_{D,obs}$, $R_{0,obs}$, and $dC/dt_{t=0}$ ratios in Table 5 would be expected to be independent. However, the fact that we can successfully fit all three ratios with only two independent parameters, α and ε, suggests that they are actually dependent and that the model may capture the basic principles of the mechanism.

The model and experiments suggest that, at equilibrium, the concentration of intramolecularly blocked ligands is approximately 15-fold that of unblocked ligands, a surprising result. The decrease in the association rate constant caused by the increase in nonbinding surface area (Janin, 1997) would scale as the square of the hydrodynamic radius (R_h). Based on the R_h values given in Table 1, this would correspond to approximately a 4-fold decrease for spherical ligands. The remainder of the 15-fold decrease is probably caused by the physical blocking of the binding site and indirect effects of PEG interactions. This implies that less than 7% of the total scFv-PEG is capable of binding the antigen at

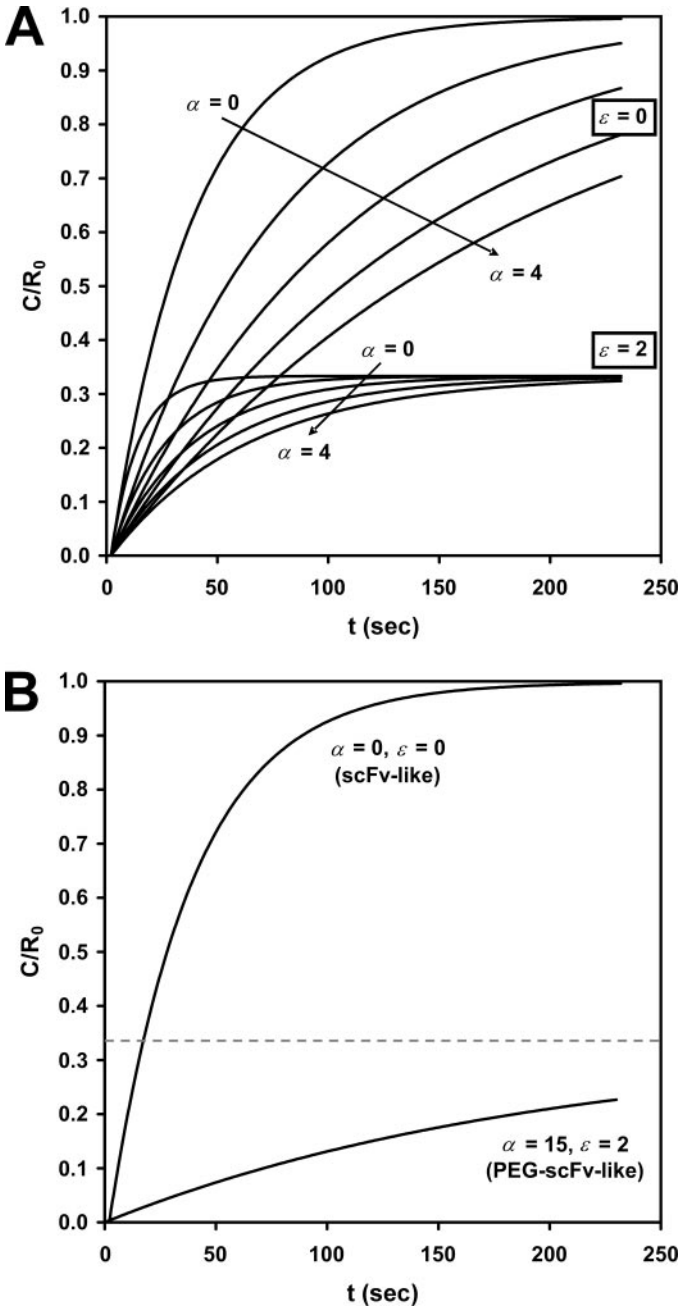

Fig. 8. Mathematical model of the influence of intramolecular (α) and intermolecular (ε) blocking on observed binding kinetics. A, the fraction of occupied binding sites (C/R_0) over time is simulated for several values of α and ε. The dependence of complex formation on α and ε can be analyzed in three phases: early-time kinetics are independent of ε; intermediate kinetics depend on both α and ε; and the equilibrium value for large L_0 [specifically $L_0 \gg (1 + \alpha)K_D/(1 + \varepsilon)$] is independent of α. B, simulated profiles of scFv-like and PEG-scFv-like ligands based on α and ε values consistent with experimental data. The dashed line at $C/R_0 = 1/3$ represents the fraction of binding sites occupied by the PEG-scFv-like ligand at equilibrium [$= 1/(1 + \varepsilon)$ where $\varepsilon = 2$; cf. eq. 15]. The kinetic parameters of the scFv monomer were used as the intrinsic rate constants for all simulations ($k_a = 3.4 \times 10^5\ M^{-1}\ s^{-1}$ and $k_d = 5.0 \times 10^{-5}\ s^{-1}$); L_0 was 78 nM [$= 100 \times (1 + \alpha)K_D/(1 + \varepsilon)$ where $\alpha = 15$ and $\varepsilon = 2$].

any given point in time, a rather counterintuitive result. However, binding to the antigen immediately displaces the rapid equilibrium; thus, all of the ligand can eventually bind to the receptor, albeit with a slower observed on rate. The off rate is identical, so a reduced affinity results. This reduced on rate resulting from intramolecular blocking is balanced by the fact that intermolecular blocking increases the apparent on rate by decreasing the apparent number of binding sites. In other words, there are far more receptors actually available for binding than the maximally observed number. For example, if $\varepsilon = 2$, the ligand molecule will bind to one antigen and then block two antigens, thus "occupying" three antigens. However, in that initial binding step, the ligand can actually bind to any of those three antigens, thus increasing the apparent association rate and consequently the apparent affinity by 3-fold, compared with a system where $R_{0,obs} = R_0$. A comparison of an unmodified monomer and a PEGylated scFv with $\alpha = 15$ and $\varepsilon = 2$ is shown in Fig. 8B.

In equilibrium cell-binding experiments, we also observed a 5-fold decrease in apparent affinity (Table 3). As mentioned previously, this effect cannot be caused by diffusion limitations, because $K_{D,obs}$ would still equal K_D at equilibrium (see eq. 8). Thus, we propose a similar dual blocking model for the binding experiments on cells. However, in this setup, the assumption of constant ligand concentration is not necessarily valid. We must modify eq. 11 to account for depletion through binding:

$$L_0 = L + L_{block} + C = L(1 + \alpha) + C \quad (16)$$

Combining eqs. 10 and 16, we can derive an expression for C at equilibrium (see Supplemental Materials):

$$C^2 - \left(L_0 + \frac{R_0}{1+\varepsilon} + \frac{1+\alpha}{1+\varepsilon}K_D\right)C + \frac{R_0}{1+\varepsilon}L_0 = 0 \quad (17)$$

A comparison of eqs. 17 and 13 clearly shows that α and ε have the same effects on $K_{D,obs}$ [$= (1 + \alpha)K_D/(1 + \varepsilon)$] and $R_{0,obs}$ [$= R_0/(1 + \varepsilon)$] as in the kinetic model of association. This is expected, because neither parameter has any effect on dissociation. Eq. 17 can easily be solved explicitly for C (see Supplemental Materials). Although the same parameter ranges proposed above for α and ε may also readily explain the observed equilibrium cell-binding assays (Table 2), we should mention that the observed maximum receptor numbers obtained in the cell-binding assays were not conclusive; furthermore, the difference in assay temperature—4°C for cell-binding assays versus room temperature for BIAcore assays—could also affect both α and ε without grossly affecting the ratio $(1 + \alpha)/(1 + \varepsilon)$, thus matching the experimental value of ~5.

From our experimental and computational analyses, it seems that neither a reduction in functional antibody concentration nor slower diffusion is responsible for the decrease in observed association rate for the PEGylated molecules. Rather, a combination of intramolecular and intermolecular blocking mechanisms can explain all of the kinetic and equilibrium binding data of these PEGylated proteins.

Discussion

Antibody-derived single-chain Fv proteins are considered a useful basis for engineering of potent anticancer therapeutics. They comprise the antigen binding specificity and affinity of monoclonal antibodies in a minimal format and can be produced in large scales in bacteria or yeast. Now they can be directly obtained from human libraries, and their binding properties and stability can further be adjusted to the requirements of an intended application by the use of rational engineering and selection strategies (see, e.g., Winter et al., 1994; Knappik et al., 2000). In tumor targeting experiments, scFv fragments showed rapid tumor localization, efficient diffusion into the tumor mass and fast systemic clearance, which leads to low background levels in healthy tissue (Adams and Schier, 1999; Batra et al., 2002). Aside from these favorable properties, however, scFv fragments have one significant drawback that limits their versatility in cancer therapy. Because their size (25 to 30 kDa) is far below the renal filtration threshold (approximately 65 kDa) (Chang et al., 1975; Maack, 1992), a major fraction of the administered molecules is removed from the blood pool before efficient accumulation at the target site can occur (Batra et al., 2002).

Today, one of the best validated strategies to enhance the serum persistence of therapeutic molecules is PEGylation—the covalent attachment of a PEG moiety. This nonimmunogenic polymer (Caliceti and Veronese, 2003) can increase the hydrodynamic radius of the conjugated protein to a huge extent, leading to significantly decreased renal clearance (Chapman et al., 1999; Lee et al., 1999; Batra et al., 2002; Chapman, 2002). Furthermore, it can act to shield protein sites from recognition by the immune system or serum proteases (Cunningham-Rundles et al., 1992; Tsutsumi et al., 2000). Because of these favorable properties, we chose PEGylation as strategy to improve the pharmacokinetic behavior of anti-p185^{HER-2} antibody fragments, which we used in tumor targeting experiments (S. Kubetzko, E. Balic, R. Waibel, U. Zangemeister-Wittke, and A. Plückthun, manu-

TABLE 5

Summary of monomer BIAcore kinetic data and mathematical models

See *Results* for details on model formulation and parameter explanation. The model parameters that are consistent with the experimental values are bold ($\alpha > 0$ and $\varepsilon > 0$). The diffusion and intramolecular blocking models cannot simultaneously explain both the k_{on} ratio and the initial association rate ($dC/dt_{t=0}$) ratio, which are observed to be different experimentally. Therefore, the latter ratio is not highlighted in either case. For the combination model, independent estimates of α and ε can be obtained from the $R_{0,obs}$ ratio and the $dC/dt_{t=0}$ ratio, respectively, and the experimental $K_{D,obs}$ and k_{on} ratios can be accurately predicted with these estimates.

	$\frac{K_{D,obs(PEG\text{-}scFv)}}{K_{D,obs(scFv)}}$	$\frac{k_{on(PEG\text{-}scFv)}}{k_{on(scFv)}}$	$\frac{k_{off(PEG\text{-}scFv)}}{k_{off(scFv)}}$	$\frac{R_{0,obs(PEG\text{-}scFv)}}{R_{0,obs(scFv)}}$	$\frac{dC/dt_{t=0(PEG\text{-}scFv)}}{dC/dt_{t=0(scFv)}}$
Experimental	5.4	0.18	0.98	0.34	0.06
Diffusion model	1	$\boldsymbol{k_t/(k_t + k_aR)}$	$k_t/(k_t + k_aR)$	1	$k_t/(k_t + k_aR)$
Intramolecular blocking model (α)	$\boldsymbol{1 + \alpha}$	$\boldsymbol{1/(1 + \alpha)}$	**1**	1	$1/(1 + \alpha)$
Intermolecular blocking model (ε)	$1/(1 + \varepsilon)$	$1 + \varepsilon$	**1**	$\boldsymbol{1/(1 + \varepsilon)}$	1
Combination model (α & ε)	$\boldsymbol{(1 + \alpha)/(1 + \varepsilon)}$	$\boldsymbol{(1 + \varepsilon)/(1 + \alpha)}$	**1**	$\boldsymbol{1/(1 + \varepsilon)}$	$\boldsymbol{1/(1 + \alpha)}$
Combination model ($\alpha = 15$ & $\varepsilon = 2$)	5.3	0.19	1	0.33	0.06

script in preparation). We constructed PEGylated variants of the monomeric scFv 4D5 (Carter et al., 1992; for review, see Willuda et al., 2001) and the dimeric miniantibody 4D5-dhlx (Willuda et al., 2001). To prevent steric interference of the 20 kDa PEG moiety with the antibody-antigen binding interaction, the polymer was site-specifically attached to a single engineered cysteine residue at the C terminus of both antibody constructs, separated by a glycine linker. Nevertheless, a decrease in functional affinity was observed when comparing the binding properties of the PEGylated constructs to their unPEGylated counterparts.

We found that PEGylation of the 4D5-derived antibody fragments led to approximately a 5-fold reduction in apparent affinity. This effect was observed in kinetic BIAcore measurements as well as in equilibrium binding assays on whole cells overexpressing the target antigen HER-2. Furthermore, the approximately 5-fold decrease in affinity was determined independently for the monovalent scFv, having one PEG molecule attached, and for the bivalent miniantibody, comprising two PEG moieties. By separate analysis of the binding kinetics, we could clearly pinpoint this effect to slower association rate constants, in that the dissociation rate constants of the antibody fragments barely changed upon PEGylation (Table 3). To better understand the molecular mechanism for the observed reduction in association rate constants, we experimentally and computationally tested several hypotheses. We could rule out a reduction in the fraction of functional molecules as a possible cause, because this value was comparable for all constructs (85–94%). Furthermore, because diffusion limitations would slow both the observed association and dissociation kinetics by the same proportion (thus leaving the observed K_D unchanged), we could also eliminate this as a means for reducing only the association kinetics of the PEGylated species. We found that the observed reduction in the association rate constant is most consistent with a combined intramolecular/intermolecular blocking mechanism. We were surprised to find that the model parameters that are representative of the experimental data suggest that less than 7% of the PEGylated antibodies in solution are capable of binding the target at any given point in time. The remaining fraction has intramolecularly blocked binding interfaces, although this dominant population is in rapid equilibrium with the functional state. This effect reduces the observed association rate constant and equilibrium affinity values but all antibody molecules can (eventually) bind to the target. In addition, the PEGylated antibodies in complexes intermolecularly block approximately two neighboring target molecules under the kinetic BIAcore conditions in the present study, thus reducing the apparent number of binding sites. However, the observed association rate constant and equilibrium affinity values are increased by this effect: because a ligand could initially bind any one of $(1 + \varepsilon)$ possible sites before then blocking the remaining ε sites with its PEG tail, the observed association rate constant is augmented by this statistical counting factor over the intrinsic association rate constant.

Although mathematical modeling of the binding kinetics of the dimer and the PEGylated dimer does not reveal any meaningful quantitative insights, because too many simplifications and assumptions would have to be introduced, we nonetheless observe some interesting trends with these molecules. It should be noted that a quantitation of the rate constants of the dimer can be only approximate, because they are not monophasic. In comparing the monomer and the dimer (Table 3), we see that the dimer has approximately a 2-fold larger observed association rate constant (because, with two binding sites, the probability of having a successful collision with the antigen is higher). Furthermore, the observed dissociation rate constant of the dimer is reduced by avidity effects (because two interaction sites have to be disrupted to release doubly bound molecules, and the singly bound dimer can bind again to form the doubly bound state). A comparison of the dimer and the PEGylated dimer reveals that the PEGylated species has a smaller k_{on}, analogous to the monomer/PEGylated monomer case. However, whereas k_{off} is unchanged when the monomer is PEGylated, k_{off} becomes larger when the dimer is PEGylated, possibly because the PEG chain intramolecularly blocks the binding of the second site in the dimer for some of the molecules. This fraction of singly bound dimers would then dissociate as monomers, thus raising the value of the observed dissociation rate constant for the PEGylated dimer.

With only two parameters, $\alpha = 15$ and $\varepsilon = 2$, the model can faithfully reproduce all of the experimental ratios in Table 5. Three of these—the $K_{D,obs}$, $R_{0,obs}$, and $dC/dt_{t=0}$ ratios—would seem, a priori, to be independent and thus should not be expected to be fit with only two parameters. The fact that they can indeed be fit in this way helps to validate the model, which predicts that these three ratios are interdependent. Our model also provides a tool for generating other testable hypotheses. For example, if the PEGylated molecule were immobilized, then the surface composition would contain a time-invariant fraction of unbound, blocked receptor (as opposed to a time-variant fraction when the PEGylated species is in solution). In such a case, the model predicts that the kinetic constants would be unaffected, whereas the observed kinetic rates would be slower because of fewer accessible binding sites. In addition, if sparser uniform coating densities of (unPEGylated) antigen could be achieved, then the intermolecular blocking component would be reduced and one should observe a decreased association rate constant, a decreased equilibrium affinity, and an increase in the number of binding sites. In addition, the model suggests that the correlation between PEG-chain size and observed association rate constant is not straightforward; rather, it results from a balance between the degree of intramolecular blocking and the degree of intermolecular blocking.

The model predicts that, in solution, more than 90% of the PEGylated ligand molecules are intramolecularly blocked. If the vast majority of the ligand is so heavily masked by the PEG moiety that accessibility to the protein is significantly hindered, this may at least partially explain the lower immunogenicity and toxicity, higher proteolytic resistance, and longer half-life often observed in vivo with PEGylated analogs. In addition, at the high concentrations often required for formulation, such masking would curtail aggregation arising from protein-protein interactions and improve solubility. This large extent of intramolecular blocking would generally not be of great concern for in vivo applications, because very high ligand concentrations ($\gg K_D$) are typically used and because the rapid equilibrium between the blocked and unblocked states would replenish any unblocked molecules that bind or become degraded. Furthermore, the positive effect of increased serum half-life on localization is

intrinsic to the PEGylation strategy. Nonetheless, if intramolecular blocking did significantly reduce the therapeutic activity of a particular ligand, the beneficial properties of PEGylation might still be realized with shorter, branched PEG moieties or by using novel coupling strategies such as reversible PEGylation (Peleg-Shulman et al., 2004).

The experiments and models presented here may help to elucidate the true mechanism(s) responsible for the reduced binding kinetics often observed with PEGylated therapeutics and, combined with other emerging insights into the effects of PEGylation (e.g., Dhalluin et al., 2005), may eventually help to tailor PEGylation to maximize the biological effect of the ligand.

References

Adams GP and Schier R (1999) Generating improved single-chain Fv molecules for tumor targeting. *J Immunol Methods* **231:**249–260.

Bailon P, Palleroni A, Schaffer CA, Spence CL, Fung WJ, Porter JE, Ehrlich GK, Pan W, Xu ZX, Modi MW, et al. (2001) Rational design of a potent, long-lasting form of interferon: a 40 kDa branched polyethylene glycol-conjugated interferon alpha-2a for the treatment of hepatitis C. *Bioconjug Chem* **12:**195–202.

Batra SK, Jain M, Wittel UA, Chauhan SC, and Colcher D (2002) Pharmacokinetics and biodistribution of genetically engineered antibodies. *Curr Opin Biotechnol* **13:**603–608.

Caliceti P and Veronese FM (2003) Pharmacokinetic and biodistribution properties of poly(ethylene glycol)-protein conjugates. *Adv Drug Deliv Rev* **55:**1261–1277.

Carter P, Kelley RF, Rodrigues ML, Snedecor B, Covarrubias M, Velligan MD, Wong WL, Rowland AM, Kotts CE, Carver ME, et al. (1992) High level Escherichia coli expression and production of a bivalent humanized antibody fragment. *Bio/Technology* **10:**163–167.

Chang RL, Ueki IF, Troy JL, Deen WM, Robertson CR, and Brenner BM (1975) Permselectivity of the glomerular capillary wall to macromolecules. II. Experimental studies in rats using neutral dextran. *Biophys J* **15:**887–906.

Chapman AP (2002) PEGylated antibodies and antibody fragments for improved therapy: a review. *Adv Drug Deliv Rev* **54:**531–545.

Chapman AP, Antoniw P, Spitali M, West S, Stephens S, and King DJ (1999) Therapeutic antibody fragments with prolonged in vivo half-lives. *Nat Biotechnol* **17:**780–783.

Christensen LL (1997) Theoretical analysis of protein concentration determination using biosensor technology under conditions of partial mass transport limitation. *Anal Biochem* **249:**153–164.

Cunningham-Rundles C, Zhuo Z, Griffith B, and Keenan J (1992) Biological activities of polyethylene-glycol immunoglobulin conjugates. Resistance to enzymatic degradation. *J Immunol Methods* **152:**177–190.

Dhalluin C, Ross A, Huber W, Gerber P, Brugger D, Gsell B, and Senn H (2005) Structural, kinetic and thermodynamic analysis of the binding of the 40 kDa PEG-interferon-alpha(2a) and its individual positional isomers to the extracellular domain of the receptor IFNAR2. *Bioconjug Chem* **16:**518–527.

Evans JW (1993) Random and cooperative sequential adsorption. *Rev Mod Phys* **65:**1281–1329.

Greenwald RB, Choe YH, McGuire J, and Conover CD (2003) Effective drug delivery by PEGylated drug conjugates. *Adv Drug Deliv Rev* **55:**217–250.

Harris JM and Chess RB (2003) Effect of pegylation on pharmaceuticals. *Nat Rev Drug Discov* **2:**214–221.

Hill RB and deGrado WF (1998) Solution structure of α_2D, a nativelike de novo designed protein. *J Am Chem Soc* **120:**1138–1145.

Janin J (1997) The kinetics of protein-protein recognition. *Proteins Struct Funct Genet* **28:**153–161.

Jeppesen C, Wong JY, Kuhl TL, Israelachvili JN, Mullah N, Zalipsky S, and Marques CM (2001) Impact of polymer tether length on multiple ligand-receptor bond formation. *Science (Wash DC)* **293:**465–468.

Johnsson B, Lofas S, and Lindquist G (1991) Immobilization of proteins to a carboxymethyldextran-modified gold surface for biospecific interaction analysis in surface plasmon resonance sensors. *Anal Biochem* **198:**268–277.

Kerwin BA, Chang BS, Gegg CV, Gonnelli M, Li T, and Strambini GB (2002) Interactions between PEG and type I soluble tumor necrosis factor receptor: modulation by pH and by PEGylation at the N terminus. *Protein Sci* **11:**1825–1833.

King DJ, Turner A, Farnsworth AP, Adair JR, Owens RJ, Pedley RB, Baldock D, Proudfoot KA, Lawson AD, Beeley NR, et al. (1994) Improved tumor targeting with chemically cross-linked recombinant antibody fragments. *Cancer Res* **54:**6176–6185.

Knappik A, Ge L, Honegger A, Pack P, Fischer M, Wellnhofer G, Hoess A, Wölle J, Plückthun A, and Virnekäs B (2000) Fully synthetic human combinatorial antibody libraries (HuCAL) based on modular consensus frameworks and CDRs randomized with trinucleotides. *J Mol Biol* **296:**57–86.

Lauffenburger DA and Linderman JJ (1993) *Receptors: Models for Binding, Trafficking and Signaling.* Oxford University Press, New York.

Lee LS, Conover C, Shi C, Whitlow M, and Filpula D (1999) Prolonged circulating lives of single-chain Fv proteins conjugated with polyethylene glycol: a comparison of conjugation chemistries and compounds. *Bioconjug Chem* **10:**973–981.

Lindmo T, Boven E, Cuttitta F, Fedorko J, and Bunn PA Jr (1984) Determination of the immunoreactive fraction of radiolabeled monoclonal antibodies by linear extrapolation to binding at infinite antigen excess. *J Immunol Methods* **72:**77–89.

Maack T (1992) Renal handling of proteins and polypeptides, in *Renal Physiology* (Windhager EE ed), *Handbook of Physiology*, *Section 8*, pp 2039–2082, Oxford University Press, New York.

Marshall SA, Lazar GA, Chirino AJ, and Desjarlais JR (2003) Rational design and engineering of therapeutic proteins. *Drug Discov Today* **8:**212–221.

Myszka DG (1999) Improving biosensor analysis. *J Mol Recognit* **12:**279–284.

Myszka DG, He X, Dembo M, Morton TA, and Goldstein B (1998) Extending the range of rate constants available from BIACORE: interpreting mass transport-influenced binding data. *Biophys J* **75:**583–594.

Northrup SH and Erickson HP (1992) Kinetics of protein-protein association explained by Brownian dynamics computer simulation. *Proc Natl Acad Sci USA* **89:**3338–3342.

O'Shannessy DJ and Winzor DJ (1996) Interpretation of deviations from pseudo-first-order kinetic behavior in the characterization of ligand binding by biosensor technology. *Anal Biochem* **236:**275–283.

Peleg-Shulman T, Tsubery H, Mironchik M, Fridkin M, Schreiber G, and Shechter Y (2004) Reversible PEGylation: a novel technology to release native interferon alpha2 over a prolonged time period. *J Med Chem* **47:**4897–4904.

Richalet-Sécordel PM, Rauffer-Bruyère N, Christensen LL, Ofenloch-Haehnle B, Seidel C, and Van Regenmortel MH (1997) Concentration measurement of unpurified proteins using biosensor technology under conditions of partial mass transport limitation. *Anal Biochem* **249:**165–173.

Slamon DJ, Godolphin W, Jones LA, Holt JA, Wong SG, Keith DE, Levin WJ, Stuart SG, Udove J, and Ullrich A (1989) Studies of the HER-2/neu proto-oncogene in human breast and ovarian cancer. *Science (Wash DC)* **244:**707–712.

Smoluchowski MV (1917) Versuch einer mathematischen Theorie der Koagulationskinetik kolloider Lösungen. *Z Phys Chem* **92:**129–168.

Tsutsumi Y, Onda M, Nagata S, Lee B, Kreitman RJ, and Pastan I (2000) Site-specific chemical modification with polyethylene glycol of recombinant immunotoxin anti-Tac(Fv)-PE38 (LMB-2) improves antitumor activity and reduces animal toxicity and immunogenicity. *Proc Natl Acad Sci USA* **97:**8548–8553.

Weir AN, Nesbitt A, Chapman AP, Popplewell AG, Antoniw P, and Lawson AD (2002) Formatting antibody fragments to mediate specific therapeutic functions. *Biochem Soc Trans* **30:**512–516.

Willuda J, Kubetzko S, Waibel R, Schubiger PA, Zangemeister-Wittke U, and Plückthun A (2001) Tumor targeting of mono-, di- and tetravalent anti-p185(HER-2) miniantibodies multimerized by self-associating peptides. *J Biol Chem* **276:**14385–14392.

Winter G, Griffiths AD, Hawkins RE, and Hoogenboom HR (1994) Making antibodies by phage display technology. *Annu Rev Immunol* **12:**433–455.

Yang K, Basu A, Wang M, Chintala R, Hsieh MC, Liu S, Hua J, Zhang Z, Zhou J, Li M, et al. (2003) Tailoring structure-function and pharmacokinetic properties of single-chain Fv proteins by site-specific PEGylation. *Protein Eng* **16:**761–770.

Address correspondence to: Andreas Plückthun, Department of Biochemistry, University of Zürich, Winterthurerstrasse 190, CH-8057 Zürich, Switzerland. E-mail: plueckthun@bioc.unizh.ch